Doctoral Dissertation

Recombinant Production of Human α-Defensin 5 via Calmodulin Fusion and Investigation of the Mechanism Enhancing Its Expression Level

（カルモジュリン融合によるヒトα-Defensin 5の組換え生産と発現レベル向上機構の解明）

Yan Shaonan

Graduate School of Life Science, Hokkaido University

2025.9

Contents

Abstract

Human α-defensin 5 (HD5), a cysteine-rich antimicrobial peptide critical for intestinal innate immunity, has been extensively studied for its structural and functional properties. Both the reduced form (HD5red) and the oxidized form (HD5oxi) exist *in vivo* and exhibit distinct antimicrobial activity spectra. In this study, we developed an efficient method to overexpress recombinant HD5 in *Escherichia coli* (*E. coli*) BL21 (DE3) strain by using calmodulin (CaM), which also interacts with antimicrobial peptides, as a fusion partner. Fusion expression suppressed the degradation of HD5 and reduced its toxicity to host cells. Following purification of the fusion protein and enzymatic cleavage to release the HD5 region, we successfully obtained sufficient amounts (yielding 1.5-1.7 mg/L culture) of active recombinant HD5oxi and HD5red for various applications, including stable isotope-label peptides for NMR analysis. Furthermore, we investigated the protective effect of CaM fusion and the mechanism of disulfide bond formation using CD and NMR spectroscopy, structural prediction, and molecular dynamics simulations. Our results suggest that the appropriate interaction strength between CaM and the HD5 region in the fusion state is a key factor for stable production.

1. Introduction

Defensins are cysteine-rich, cationic, and amphipathic peptides, typically 2–5 kDa in size, stabilized by intramolecular disulfide bonds. They constitute a major class of antimicrobial peptides (AMPs) found in humans, mice, insects, and plants, and play an essential role in the initial defense mechanism of the host immune system against microbial invasion [1]–[3]. Human defensins are classified into two main subfamilies, α- and β-defensins, based on sequence similarity and distinct disulfide bond patterns, with both forming β-sheet-rich structures. α-Defensins follow a CysI–CysVI, CysII–CysIV, and CysIII–CysV disulfide connectivity pattern and are primarily found in neutrophils (human neutrophil peptides, HNPs 1–4) and intestinal Paneth cells (human α-defensins, HD5 and HD6), whereas β-defensins adopt a CysI–CysV, CysII–CysIV, CysIII–CysVI configuration and are predominantly expressed in epithelial cells [4]–[7].

Among the six human α-defensins, HD5 exhibits the most potent and broad-spectrum antibacterial activity against both Gram-positive and Gram-negative bacteria [8]–[10], serving as a critical component of the human intestinal innate immune system [11][12]. The oxidized form of HD5 (HD5oxi), featuring three disulfide bonds, forms an antiparallel β-sheet structure typical of α-defensins, with these disulfide bonds being essential for structural stability and biological function [8][13]. In contrast, the fully reduced form (HD5red), lacking disulfide bonds, exhibits weakened antimicrobial activity against *Staphylococcus aureus* (*S. aureus*) [14], while its binding capacity to

lipopolysaccharide (LPS) is increased, suggesting a potential anti-inflammatory role [8]. Recently, HD5red has been detected in the human intestinal tract—a highly reducing environment—further drawing attention to its physiological role [15][16]. However, the relationship between structural changes and functional characteristics in HD5 remains poorly understood. Techniques such as nuclear magnetic resonance (NMR) spectroscopy, which provide insights into three-dimensional structures and molecular interactions, are therefore considered highly valuable. Against this backdrop, developing an efficient method for producing stable isotope-labeled HD5 via recombinant overexpression is crucial.

Escherichia coli (*E. coli*)-based recombinant protein expression offers several advantages, including compatibility with various vectors, high-density cultivation, and low production costs [17]. However, small peptides like AMPs are more prone to proteolytic degradation in host cells compared to larger, more stable proteins [18]. Various strategies have been employed to enhance the stability and expression levels of AMPs, including members of the defensin family. For HD5, successful expression as inclusion bodies by adding a 6× histidine (His) tag to the N-terminus has been reported [10][14]. Nevertheless, this approach requires complex refolding procedures to correctly form disulfide bonds [19][20]. Another widely used strategy involves expressing the target peptide as a fusion protein with a carrier protein, and various fusion partners have been explored for this purpose [18][21][22].

Recently, calmodulin (CaM) has been investigated as a fusion partner for recombinant

AMP expression [23][24]. CaM possesses a dumbbell-shaped structure comprising two globular lobes connected by an α-helix, and undergoes conformational changes in response to Ca^{2+} concentration, enabling it to wrap around positively charged amphipathic helices in target proteins [25]–[28]. Although AMPs are not natural binding targets for CaM, several—including fowlicidin-1 (Fow1) and cecropin P1 (CP1)—share structural features similar to typical CaM-binding motifs and exhibit strong interactions with CaM [29]. This binding appears to confer protection during recombinant expression, facilitating the production of α-helical AMPs as fusion proteins [24][29]. Based on these properties, CaM's utility as a fusion partner was initially thought to be limited to α-helical AMPs. However, successful CaM-fusion expression has also been demonstrated for AMPs with β-sheet structures stabilized by disulfide bonds, such as macrophage inflammatory protein 3α (MIP-3α) [30] and human β-defensin 3 (HBD-3) [24]. In these cases, the *E. coli* Origami strain, which provides an oxidative intracellular environment conducive to disulfide bond formation, was used successfully. Notably, strong interactions between CaM and the target peptide could potentially inhibit disulfide bond formation, highlighting the need to balance protective effects and oxidative folding. Therefore, producing HD5oxi via CaM fusion offers a valuable opportunity to gain insights into these competitive processes.

In this study, we investigated the recombinant expression of HD5 fused to CaM. The fundamental characteristics of CaM and HD5 are summarized in **Table 1**. We confirmed that CaM fusion enabled the expression of functional HD5oxi and allowed the efficient

preparation of stable isotope-labeled samples suitable for NMR analysis. Furthermore, we explored the underlying mechanism of recombinant expression of β-sheet peptides fused to CaM through experimental approaches using recombinant HD5 and molecular dynamics simulations.

2. Martials and methods

2.1 Vector construction

The HD5 gene segment was amplified by polymerase chain reaction (PCR) using a specific set of primers. Subsequently, the amplified product was ligated into the pET15b-CaM-enterokinase (EK) vector, which had been double-digested with *Kpn*I and *Xho*I restriction enzymes, according to a previously established method in our laboratory [29]. The newly constructed vector, designated pCaM-EK-HD5, features an N-terminal 6×His-tag and is controlled by a T7/lac promoter. In this study, *E. coli* DH5α (Novagen) was used for plasmid storage and template preparation. The restriction enzymes FastDigest® *Xho*I and *Kpn*I (Thermo Fisher Scientific) were used. DNA extraction and purification were performed using the FastGene® Plasmid Mini Kit (NIPPON Genetics Co., Ltd).

2.2 Overexpression of CaM-HD5 in *E. coli*

E. coli BL21(DE3) (Novagen) and *E. coli* Origami™ B (DE3) (Novagen) competent cells were transformed with pCaM-EK-HD5. Transformants were cultured in 5 mL of lysogeny broth (LB) medium supplemented with 50 μg/mL carbenicillin at 37°C. Upon reaching an absorbance of 0.6–0.8 at 600 nm, the cultures were induced with 1 mM IPTG and incubated with shaking at 180 rpm for 4 h. Cell pellets from 1 mL of bacterial culture were lysed by manual sonication in Tris-HCl buffer (pH 8.0). Following centrifugation at 15,000 rpm for 3 min, the lysates were analyzed by 15% SDS-PAGE.

For large-scale expression of CaM-HD5, 1 L of M9 minimal medium was used for culturing *E. coli* BL21(DE3) cells. For preparation of ^{15}N-labeled peptides, M9 medium containing 2 g/L $^{15}NH_4Cl$ as a nitrogen source was used; for ^{15}N,^{13}C-labeled peptides, 1 g/L ^{13}C-glucose was additionally added as a carbon source, following the same procedures. The components of the M9 medium, including a 100× BME vitamins mixture (Sigma-Aldrich Inc.), are listed in **Table S1**. Cells cultured in different media followed similar experimental procedures.

After overnight culturing in 50 mL of medium containing 50 μg/mL carbenicillin at 37°C, the cells were harvested by centrifugation at 6,000 rpm for 5 min, equally divided, and resuspended in 500 mL of fresh medium with 50 μg/mL carbenicillin in two flasks. Bacterial cells were induced with 1 mM IPTG at the same growth stage as described above and further cultured for an additional 4 h. Cell pellets were collected by centrifuging aliquots of the culture hourly after induction at 13,000 rpm for 3 min. After disrupting the cell pellets using a sonicator (Misonix MICROSON Ultrasonic Cell Disruptor XL2000), both the pellet and supernatant obtained after centrifugation at 15,000 rpm for 5 min were analyzed by 15% SDS-PAGE and tricine SDS-PAGE. The gels were stained using EzStain Aqua (ATTO Corporation).

2.3 Purification, enzymatic digestion, and molecular analysis

Cell pellets from large-scale overexpression were collected by centrifugation at 6,000

rpm for 10 min at 4°C and resuspended in binding buffer for immobilized metal affinity chromatography (IMAC) (20 mM Tris-HCl, 300 mM NaCl, pH 8.0). Cells were lysed using an ultrasonic disruptor (Insonator 201 M, KUBOTA) at 180 W for 30 min. Following centrifugation of the lysate at 7,500 rpm for 20 min, the supernatant was recovered and filtered through a Millipore Millex-HV 0.45 μm filter (Merck). The samples were subsequently purified by one-step IMAC. Each sample solution was applied to a Ni-NTA column (Thermo Fisher Scientific) pre-equilibrated with washing buffer (20 mM Tris-HCl, 20 mM imidazole, 300 mM NaCl, pH 8.0) at a volume of five times the column volume. The CaM-HD5 fusion proteins were eluted using elution buffer (20 mM Tris-HCl, 300 mM imidazole, 300 mM NaCl, pH 8.0) at five times the column volume, followed by a wash with buffer containing 500 mM imidazole. All fractions and flow-through from the IMAC were analyzed by 15% SDS-PAGE.

The fractions containing the majority of the fusion proteins were further dialyzed against 20 mM Tris-HCl buffer (pH 8.0) at room temperature for 12 h. Following centrifugation at 6,000 rpm for 10 min, the concentration of the fusion proteins in the supernatant was determined by UV absorption at 280 nm. EK digestion trials were conducted by varying reaction temperature, protease concentration, reaction time, and assessing the effects of pH and the presence of EDTA. After optimizing and comparing HD5 recovery under various conditions using tricine SDS-PAGE, the dialyzed fusion protein samples were incubated in EK digestion buffer (50 mM Tris-HCl, 1 mM $CaCl_2$, 0.1% Tween-20, pH 8.0) with 1 U/mL EK protease (EKMax, Thermo Fisher Scientific) at 22°C for 20 h

without EDTA. After EK digestion, samples were centrifuged at 10,000 rpm for 2 min, the pH was adjusted to 2–3 using 10% trifluoroacetic acid (TFA), and then filtered through a Millex-HV 0.22 μm filter (Merck).

Subsequent purification was carried out by RP-HPLC on a COSMOSIL 5C18 AR-300 column (Nacalai Tesque) using a linear gradient of 10–60% acetonitrile (ACN) containing 0.1% TFA. The retention time of HD5oxi was confirmed by comparing it with a chemically synthesized peptide (Peptide Institute, Inc.) under the same RP-HPLC conditions. Peptide yields were determined by measuring absorbance at 280 nm.

For the preparation of HD5red, one approach involved directly reducing the EK-treated fusion protein solution by adding 150–200 mM dithiothreitol (DTT) and incubating for 1–2 h at room temperature, followed by RP-HPLC purification as described above. Alternatively, lyophilized HD5oxi and intermediate fractions from RP-HPLC were reduced with 200 mM DTT overnight at room temperature, and subsequently purified by RP-HPLC. The molecular weights of both the purified oxidized and reduced forms of HD5 were confirmed by MALDI-TOF mass spectrometry (Autoflex Speed, Bruker). Acid-urea PAGE (AU-PAGE) was performed as previously described [31].

2.4 *In vitro* refolding

HCl buffer (pH 8.0) at room temperature for 12 h to remove salts and chemical reagents. Subsequently, the samples were dialyzed against refolding buffer (20 mM Tris-HCl, pH

8.0, 200 mM NaCl, 2 M urea, 3 mM reduced glutathione, and 0.3 mM oxidized glutathione) at 4°C for 12–18 h [32], with the dialysis process repeated twice to test refolding efficiency. Finally, the samples were dialyzed overnight against 20 mM Tris-HCl buffer (pH 8.0) again to remove any remaining additives prior to EK digestion. EK digestion and subsequent RP-HPLC purification were performed using the same procedures as in the non-refolded group.

2.5 Antibacterial activity assay

The antimicrobial activity of recombinant HD5oxi against *S. aureus* (ATCC 6538p) and *E. coli* (ATCC 43827) was evaluated using previously published broth microdilution method in 96-well plates [9][33][34]. Peptides purified by RP-HPLC were lyophilized and reconstituted in 10 mM sodium phosphate buffer (SPB, pH 7.4) to prepare a series of 2× concentrated solutions, and 50 μL of the solutions was placed in each well, resulting in final peptide concentrations ranging from 32 to 0.5 μM upon mixing with the bacterial suspension. For bacterial suspension, single colonies of two types of bacteria were inoculated into 5 mL of Mueller–Hinton Broth (MHB) and cultured at 37°C for 2 to 6 hours to reach the mid-log phase. The bacterial cells were then washed and resuspended in SPB to prepare a suspension of 1-2 × 10^6 CFU/mL, and 50 μL of this suspension was added to each well containing peptide solution, achieving a final concentration of 5 × 10^5 CFU/mL per well. The concentration of the cell control group (without peptides) was

confirmed by plating the inoculum onto MHB agar and counting colony-forming units.

After incubation for 2-3 h at 37 °C, 100μL of fresh medium was added into each well and incubated at 37°C for an additional 16-20 h with vigorous shaking. The bacterial growth was evaluated by reading at 600 nm using a microplate reader (Benchmark Plus, Bio-Rad). The lowest concentration of peptides that inhibited bacterial cell without visible growth was defined as the minimal inhibitory concentration (MIC). The MICs were obtained in three independent measurements.

2.6 NMR analysis

Recombinant ^{15}N-labeled HD5oxi and HD5red peptides were produced following the expression and purification protocols described above. For NMR sample preparation, 0.2 mM of either HD5oxi or HD5red peptides obtained after RP-HPLC purification and lyophilization were dissolved in a 90% H_2O/10% D_2O mixture at pH 4.0, adjusted with minimal amounts of HCl or NaOH. For the NMR sample of the HD5red–CaM complex, a stock solution of non-labeled CaM was mixed with 0.15–0.2 mM ^{15}N-HD5red dissolved in sterile water at various molar ratios, maintaining the pH at 4.0. The non-labeled CaM, bearing a 6×His-tag, was prepared using similar expression and purification procedures. All heteronuclear single quantum correlation (HSQC) spectra were acquired at 298 K on a Bruker AVANCE III HD 600 MHz spectrometer equipped with a 5 mm TXI probe with x-, y-, and z-axis gradients. All HSQC spectra were processed using TopSpin software

and analyzed using Sparky.

2.7 Circular dichroism (CD) spectrometry

Each sample of HD5red (final concentration: 0.1 mg/mL, 27.8 μM) was measured in 10 mM sodium phosphate buffer (pH 7.4) under both aqueous conditions and in the presence of 40% TFE. Measurements were performed using a J-725 spectropolarimeter (JASCO) equipped with a 0.1 cm path-length quartz cell. Spectra were acquired over a wavelength range of 260–190 nm, using a bandwidth of 0.2 nm, a response time of 1 second, and a data interval of 0.2 nm. Scans were performed at a rate of 20 nm/min at 25°C, with each sample measured three times under a nitrogen gas atmosphere. Following the measurements, the spectrum of 10 mM sodium phosphate buffer (pH 7.4) was subtracted. Molar ellipticity ([θ]) was calculated using the following formula:

$$[\theta] = \frac{\theta_{observed}}{10 \times n \times C \times l}$$

where n is the number of amino acid residues, C is the molar concentration of the peptide, and l is the optical path length of the cell (cm).

2.8 AlphaFold predictions

The structural models of the CaM-HD5 fusion protein were predicted using AlphaFold2 on the publicly available Colab server [35]. Predictions were conducted using the default settings. Templates were not used, and multiple sequence alignments were generated

using the MMSeqs2 server. The number of recycles was set to 48, and no structural relaxation was performed after prediction. The full-length protein sequences encoded by pCaM-EK-HD5 and, for comparison, pCaM-TEV-Fow1 [24], were used as inputs, and the most favorable models were selected as representative results. Molecular graphics were visualized using PyMOL (Schrödinger, LLC, 2010; The PyMOL Molecular Graphics System, Open-Source Version 3.0.0).

2.9 Molecular dynamics (MD) simulation

MD simulations were performed using GROMACS (version 2020.3) (https://doi.org/10.5281/zenodo.10589697) [36], with AlphaFold-predicted structures as the initial models. The CHARMM-GUI server [37] was used to generate input files for GROMACS. AlphaFold-predicted structures were embedded in a simulation box with an initial size of 114 × 114 × 114 Å³ using the Solution Builder module of the CHARMM-GUI server. The system was solvated with TIP3P water and 150 mM sodium chloride. According to CHARMM-GUI guidelines, all histidine residues were modeled as neutral, while other basic and acidic residues retained their standard charges. The CHARMM36m force field [38] was used for all simulations.

Energy minimization was performed using the steepest descent algorithm for 5,000 steps. The system was equilibrated for 125 ps under NVT conditions at 298 K using a V-rescale thermostat. Production MD simulations were conducted for 200 ns with a 2-fs time step

under periodic boundary conditions at 298 K and 1 bar using a Parrinello–Rahman barostat. Long-range electrostatics were treated using the Particle Mesh Ewald (PME) method [39] with a direct space cutoff of 12 Å. The LINCS algorithm was applied to constrain all bonds involving hydrogen atoms. Structural stability and dynamics were assessed by calculating root mean square deviation (RMSD) and root mean square fluctuation (RMSF). The MD simulation results were visualized using VMD [40] and PyMOL software.

3. Results

3.1 Expression of recombinant HD5 in the CaM fusion state

Following the strategy used in previous studies for constructing CaM fusion protein expression systems with other antimicrobial peptides [24][29], we designed a vector containing a 6×His-tag sequence followed by the CaM-HD5 fusion protein, with an EK cleavage site (DDDDK-X) inserted between the two regions. The primary structure of HD5 and the constructed vector, designated pCaM-EK-HD5, are shown in **Fig. S1**. The CaM-HD5 fusion protein was overexpressed in *E. coli* BL21(DE3) through IPTG induction under the control of the T7/lac promoter. To facilitate the production of stable isotope-labeled peptides for heteronuclear NMR studies, cultivation and overexpression were conducted in M9 minimal medium. In both ^{15}N single-labeled and ^{15}N,^{13}C double-labeled media, IPTG induction of CaM-HD5 had no impact on cell growth (**Fig. 1a, Fig. S2a**). Tricine SDS-PAGE analysis confirmed that the fusion protein was highly expressed in a soluble form, demonstrating the robustness and scalability of this expression system (**Fig. 1b, Fig. S2b**). The role of CaM in increasing yields and reducing cytotoxicity of HD5 was further confirmed via a side-by-side comparison in **Fig. S3**. Additionally, compared to other CaM-fused AMPs such as Fow1, CP1, and human cathelicidin LL-37, CaM-HD5 showed lower cytotoxicity and higher expression efficiency (**Fig. S4**). The Origami B (DE3) strain, which provides an oxidative environment favorable for disulfide bond formation, was also used. However, it showed a lower expression level compared

to the BL21 (DE3) strain **(Fig. S5)**. Thus, we selected BL21(DE3) as the host strain for continued production of CaM-HD5 fusion proteins.

3.2 Purification and enzymatic cleavage of CaM-HD5

The CaM-HD5 fusion protein was recovered from the supernatant of sonicated *E. coli* lysates and purified via one-step IMAC. To improve peptide stability and minimize degradation during IMAC, a high concentration of NaCl was included. The fusion proteins were successfully eluted with minimal degradation, as confirmed by SDS-PAGE (**Fig. S6**). Approximately 30 mg of ^{15}N-labeled CaM-HD5 (~23.7 kDa) was obtained from 1 L of culture. The eluted fusion proteins were dialyzed to remove imidazole, and the entire purification process was monitored by SDS-PAGE **(Fig. 2)**.

The dialyzed fusion protein was treated with EK under various conditions to cleave the HD5 domain **(Fig. S7)**. Following optimization, the optimal cleavage conditions (20 hours at 22°C with 1 U/mL enzyme) achieved maximal HD5 recovery while minimizing precipitation and non-specific cleavage (**Fig. 3**).

Following EK treatment, the cleaved peptides were purified by RP-HPLC (**Fig. 4a**). Non-reducing tricine SDS-PAGE analysis (**Fig. 4b**) showed that the fraction eluting at 30–31 minutes matched the retention time of chemically synthesized HD5oxi. Additionally, MALDI-TOF mass spectrometry confirmed the mass corresponding to HD5oxi (**Table 2**), and AU-PAGE analysis further supported correct disulfide bond

formation (**Fig. S8**). Despite the reducing environment of BL21(DE3) and the absence of *in vitro* refolding steps, 1.2–1.5 mg of ^{15}N-HD5oxi was obtained per 1 L of culture—a yield significantly higher than previously reported insoluble expression strategies [10]. Subsequently, for comparison and further studies, ^{15}N-HD5red was also produced in this system by directly reducing the EK-treated solution. It was purified by RP-HPLC under the same conditions, eluting at approximately 39 minutes (**Fig. S9**), and was further characterized by MALDI-TOF analysis (**Table 2**). These results confirmed that HD5red can also be efficiently obtained.

Most of the HD5 obtained from the CaM fusion overexpression system possessed correct disulfide bonds without requiring special *in vitro* refolding treatment; however, a small population of intermediate molecular species was still detected (**Fig. 4**). To investigate whether these intermediates within the fusion protein could be further folded to increase the proportion of correctly folded molecules, we performed an additional procedure without any prior reduction treatment. After dialysis, EK digestion, and RP-HPLC purification, the yield increased to 1.5–1.7 mg of correctly folded ^{15}N-HD5oxi per liter (**Fig. S10**). Extended dialysis (12 h) showed no significant improvement over standard refolding conditions.

3.3 Antibacterial activity assay of recombinant HD5

To confirm that our recombinant HD5oxi obtained from the CaM-HD5 fusion system,

exhibited the expected antibacterial activity, we conducted a broth microdilution assay against the Gram-positive bacterium *S. aureus* and the Gram-negative bacterium *E. coli* (both at 5×10^5 CFU/mL). As summarized in **Table 3**, recombinant HD5oxi demonstrated antibacterial activity. Inhibitory effects were observed at 4 μM and 1 μM, respectively, with no visible growth of *E. coli* and *S. aureus*. These findings are consistent with previous reports showing that HD5oxi exhibits antimicrobial activity against *S. aureus* and *E. coli* at low concentrations using identical methodology [9][33].

3.4 Three-dimensional structure of HD5 and its interaction with CaM

To further evaluate the structural integrity of recombinant HD5oxi, we performed HSQC NMR spectroscopy, which provides information on protein folding states [41]. The efficient production of ^{15}N-labeled HD5 enabled detailed NMR analysis. The 2D ^{1}H-^{15}N HSQC spectra of ^{15}N-HD5oxi and ^{15}N-HD5red in water are shown in **Fig. 5a and 5b**. For HD5oxi, well-dispersed cross-peaks corresponding to main-chain amide signals, along with consistency with previously reported spectra [10], indicated that the recombinant HD5oxi adopted the correct disulfide bond pattern and native structure. The ^{1}H–^{15}N HSQC chemical shifts of HD5oxi are summarized in Table S2. These values are overall consistent with previously data reported in the BMRB (https://bmrb.io, Entry ID: 18705). In contrast, HD5red showed signals clustered around 8.0–8.5 ppm for ^{1}H, suggesting a random coil conformation.

To investigate the possibility of interactions between CaM and HD5 in the intracellular reducing environment that may contribute to the protection and expression, we measured the ^{1}H-^{15}N HSQC spectra of mixtures of ^{15}N-HD5red and unlabeled CaM (**Fig. 5c**). Slight chemical shift changes and intensity reductions were observed for some signals, but no strong binding pattern was detected, contrasting with Fow1, which forms α-helices upon binding to CaM [24].

3.5 Structural prediction and molecular dynamics analysis in CaM fusion states

Although no clear strong interaction was observed experimentally, we performed computational structural prediction to further elucidate the mechanism by which CaM-fused HD5 is stably expressed as a recombinant protein. First, we predicted the structure of Fow1 in the CaM fusion state using AlphaFold2 [42]. Each model generated by AlphaFold2 was ranked based on internal confidence metrics, such as predicted Local Distance Difference Test (pLDDT) scores, which represent the reliability of predictions for each residue (**Fig. 6, Fig. S11**). In all five predicted structures (ranks 1 to 5), the N-lobe (residues 21–93) and C-lobe (residues 102–168) of CaM, as well as the Fow1 region (residues 178–203), exhibited relatively high pLDDT values, indicating high prediction reliability. A common feature across all structures was that Fow1 formed an amphipathic α-helix deeply enclosed by the N- and C-lobes of CaM, following the typical "wrap-around" or "clamp-like" binding mode seen in recognition of CaM target sequences

[43][44]. The two lobes of CaM wrapped around the Fow1 helix at an angle of approximately 90°, closely resembling previously reported NMR structures of CaM–MLCK, CaM–CaMKK[45], and CaM–PMCA [46] complexes. The Trp6 and Leu19 residues of Fow1 were inserted into the hydrophobic pocket of CaM in a typical "1–14 binding motif" (hydrophobic residues at positions i and i+13) [45], supporting the structural reliability of the predictions.

Similarly, the structural predictions for CaM-HD5 (ranks 1 to 5) showed high pLDDT scores for the CaM domains (**Fig. S12**), consistent with the results for CaM-Fow1. However, the HD5 region (residues 178–209) displayed low pLDDT scores and greater variability among the models (**Fig. 7**). In structures ranked 1 to 3, the HD5 region was not enclosed by CaM and was positioned distantly without clear interaction. These HD5 regions mostly exhibited random conformations, although in the rank 2 model, CysI and CysVI were positioned close together, and a short β-sheet comprising two antiparallel β-strands, resembling the structure of oxidized HD5 (HD5oxi), was observed. Notably, in ranks 4 and 5, HD5 showed interaction with CaM and was partially enclosed. In the rank 4 model, the HD5 region clearly formed an α-helix, similar to Fow1 in CaM-Fow1 complexes. However, the distance between the two CaM lobes in CaM-HD5 (31.6 Å) was slightly wider than that in CaM-Fow1 (22.4 Å), suggesting that CaM-Fow1 may adopt a more stable structure.

To further assess the stability of these predicted structures, we conducted 200-ns molecular dynamics (MD) simulations (**Fig. 8**). In the rank 1 structure, where the HD5

region did not interact with the CaM region, large root-mean-square fluctuation (RMSF) values in the HD5 region indicated high flexibility throughout the MD simulation (**Fig. 8a**), as also confirmed by structural snapshots (**Fig. 8b**). Conversely, the rank 4 model, where HD5 formed an α-helix and interacted with CaM, exhibited low RMSF values across the entire fusion protein, indicating that the structure was sufficiently stabilized by interactions (**Fig. 8c, 8d**).

3.6 Evaluation of helix formation ability of HD5red using CD spectroscopy

To experimentally evaluate the structural properties of HD5red that may contribute to interaction with CaM, we evaluated the α-helix-forming potential of HD5red using CD spectroscopy (**Fig. S13a**). HD5red exhibited a random coil spectrum in aqueous solution with a negative peak near 200 nm, but upon addition of the hydrophobic solvent 2,2,2-trifluoroethanol (TFE), the spectrum showed negative peaks at approximately 208 nm and 222 nm, characteristic of α-helical structure. This finding suggests that HD5red has an intrinsic propensity to adopt α-helix structures in hydrophobic environments such as protein–protein interfaces. Further analysis using a helical wheel model revealed that the α-helical form of HD5red possesses an amphipathic structure with a hydrophobic surface, a typical feature recognized by CaM (**Fig. S13b**).

4. Discussion

Numerous studies have highlighted the importance of selecting an appropriate expression format to balance production efficiency, structural integrity, and functional activity of recombinant AMPs [18][22]. The challenges in expressing defensins in *E. coli* have been well documented, particularly the need for a fusion partner that can prevent degradation and reduce toxicity. Successful expression of human β-defensins (HBD-2~HBD-6) has been achieved using thioredoxin A (TrxA) as a fusion partner which is recognized for enhancing soluble expression of various AMPs in *E. coli* [21]. Notably, CaM fusion has been shown to facilitate expression more effectively than other soluble tags, in part due to CaM's smaller size [29][30]. Successful expression of disulfide bond-stabilized AMPs such as HBD-3, which shares a β-sheet structure similar to HD5, has also been reported [24]. Consistent with these findings, our results of recombinant expression indicated that CaM fusion can effectively enable high levels of soluble HD5 expression (**Fig. 1, Fig. S2**). Previous studies have shown that CaM fusion reduces AMP-induced toxicity in host cells, as demonstrated with Fow1 [24] and CP1 [29]. A side-by-side comparison of CaM-HD5 fusion, CaM alone, and non-fused HD5, expressed in *E. coli* BL21(DE3) under identical conditions, showed that IPTG-induced expression of non-fused HD5 caused significant toxicity to host cells, and almost no soluble expression was observed after cell lysis. In contrast, CaM fusion effectively overcame these challenges (**Fig. S3**). These results highlight the ability of CaM fusion to reduce the

cytotoxicity of HD5 and enhance its expression level. Furthermore, compared to Fow1, CP1, and human cathelicidin LL-37, CaM-HD5 exhibited superior mitigation of cytotoxicity while maintaining high overexpression levels **(Fig. S4)**.

Proper disulfide bond formation is crucial for defensins. Although our results showed that CaM fusion enhanced HD5 expression in BL21(DE3), disulfide bond formation remained a challenge. To address this, we evaluated expression in the Origami B strain, which provides an oxidative intracellular environment [30][32]. However, SDS-PAGE analysis revealed no detectable soluble fusion protein production in Origami B (**Fig. S5**), in contrast to successful expression of HBD-3 [24] and MIP-3α [30]. One possible explanation is that HBD-3 and MIP-3α contain additional helical regions absent in HD5, facilitating CaM binding and enhancing solubility even in oxidative hosts. Furthermore, previous studies showed that HD5 fused to GFP exhibited significantly lower soluble yields in Origami B compared to BL21(DE3) [47].

After successful expression and purification of the CaM-HD5 fusion proteins, we next focused on optimizing the enzymatic cleavage conditions required to efficiently release the HD5 domain for downstream applications. Cleavage efficiency was found to be higher at temperatures below room temperature, consistent with previous reports for cryptdin-2 expressed using a Trx fusion system [48]. Based on this observation, various factors, including temperature, pH, enzyme concentration, and reaction time, were tested to determine the optimal conditions for EK digestion. As a result, the optimized conditions achieved the highest cleavage efficiency for isolating and recovering HD5 compared to

other tested conditions (**Fig. S7**). Stronger cleavage conditions did not further improve digestion efficiency, possibly due to heterogeneity in disulfide bond formation.

In fact, during purification process, treatment with a reducing agent significantly reduced the intensity of the dimeric band (~47.4 kDa) on SDS-PAGE (**Fig. 2**), suggesting that a minor population formed intermolecular disulfide bonds, while the majority existed as monomers. Although this observation does not directly constitute evidence of correct folding, it suggests that disulfide bond formation occurred during the early stages of purification. We speculate that oxidative folding primarily took place during cell lysis by sonication, a step known to expose proteins to atmospheric oxygen. This speculation is supported by previous studies, which recommend the use of reducing agents during cell lysis to prevent unintended oxidation and disulfide bond formation in similar situations [49].

The main fraction obtained from RP-HPLC following EK digestion exhibited a retention time consistent with the chemically synthesized HD5oxi. However, because no *in vitro* refolding step was performed, we carefully investigated whether this fraction had indeed adopted the native oxidized conformation, we carefully investigated whether this fraction had indeed adopted the native oxidized conformation. Mass spectrometry analysis confirmed the correct molecular weight corresponding to fully oxidized HD5, and AU-PAGE showed identical mobility to a chemically synthesized HD5oxi standard, supporting proper disulfide bond formation and native folding. AU-PAGE mobility is highly sensitive to the three-dimensional structure of defensins; it has been reported that

if the native structure is disrupted, for example by incorrect disulfide bond formation, the mobility differs significantly [31].

The correct folding of recombinant HD5oxi was further evaluated by antibacterial activity measurements and NMR spectroscopy. Given the known limitations of Mueller–Hinton Broth (MHB) as the sole incubation medium in evaluating the activity of cationic AMPs [50], we adopted a protocol from previous studies of human defensins, which involved pre-incubating peptides and bacterial cells in a low-salt SPB buffer before the addition of MHB. This modified approach better preserves the activity of peptides during the early interaction phase with bacterial membranes. Using this method, we observed potent activity of HD5oxi at low micromolar concentrations against both *E. coli* and *S. aureus*, in line with previous reports with minor differences likely due to strain variation.

Despite being expressed in the reducing environment of BL21(DE3) cells, HD5oxi was successfully obtained without special refolding steps. Therefore, this oxidation is presumed to have occurred in the oxidative environment of the purification process. It is notable to consider how HD5red, presumably adopting a random coil conformation intracellularly, interacted with CaM to avoid degradation. Previous studies suggested that CaM protects AMPs primarily by binding to their α-helical structures [24]. Additionally, if CaM interacts with HD5red, it is intriguing to understand why this interaction does not inhibit the extracellular formation of disulfide bonds during purification. However, the HSQC spectra indicated no strong interactions between HD5red and CaM, as evidenced by the absence of significant chemical shift changes (Fig. 5c). Although the NMR

experiments using mixtures of CaM and HD5red did not reveal strong interactions or structural changes, structural prediction and MD simulations suggested that in the fusion state, weak interactions and partial α-helix formation in HD5 might occur. Consistently, CD spectroscopy also indicated that propensity of HD5red to form α-helix. The combined computational and experimental results provide mechanistic insight into the role of CaM in expression of HD5. Of course, it cannot be entirely ruled out at this stage that CaM-HD5 exerts a protective effect that enhances expression efficiency without involving specific interactions, similar to other common soluble fusion tags [21]. The recombinant production system established in this study for CaM-HD5 fusion proteins, HD5red, and HD5oxi provides a powerful platform not only for elucidating the antibacterial mechanism of HD5, which is still not fully understood, but also for advancing our understanding of CaM fusion-enhanced expression systems.

5. Conclusion

In this study, we demonstrated that HD5 fused with CaM can be efficiently recombinantly expressed in a soluble form using *E. coli* as a host. This method was applicable to both the oxidized form (HD5oxi) and the reduced form (HD5red), and stable isotope-labeled samples for NMR studies were efficiently prepared. Furthermore, we showed that disulfide bond formation, which is necessary for the conversion of reduced HD5red to oxidized HD5oxi, is not inhibited even in the CaM fusion state. Insights into the interactions and structures between CaM and the target peptides may provide important clues for extending the CaM fusion expression system to the production of other AMPs and peptide classes.

6. Figures & Tables

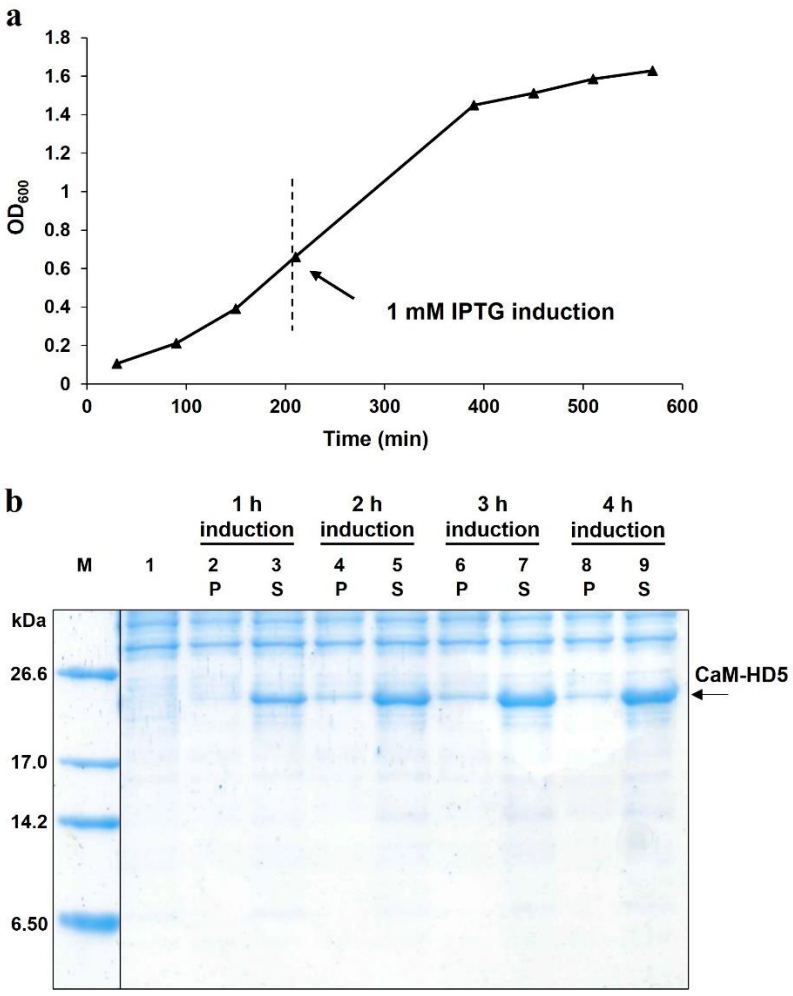

Fig. 1. Overexpression of ^{15}N-labeled CaM-HD5. (**a**) Growth curve of BL21(DE3) cells expressing ^{15}N-CaM-HD5 in M9 medium, induced with 1 mM IPTG at an OD_{600} of approximately 0.6–0.8. (**b**) Tricine SDS-PAGE analysis of lysed cell pellets following induction with 1 mM IPTG. Lane M: Molecular weight marker; Lane 1: Whole cells before induction; Lanes 2–3, 4–5, 6–7, and 8–9: Lysed cells after 1, 2, 3, and 4 hours of IPTG induction, respectively. P, S: Pellet and supernatant after centrifugation, respectively.

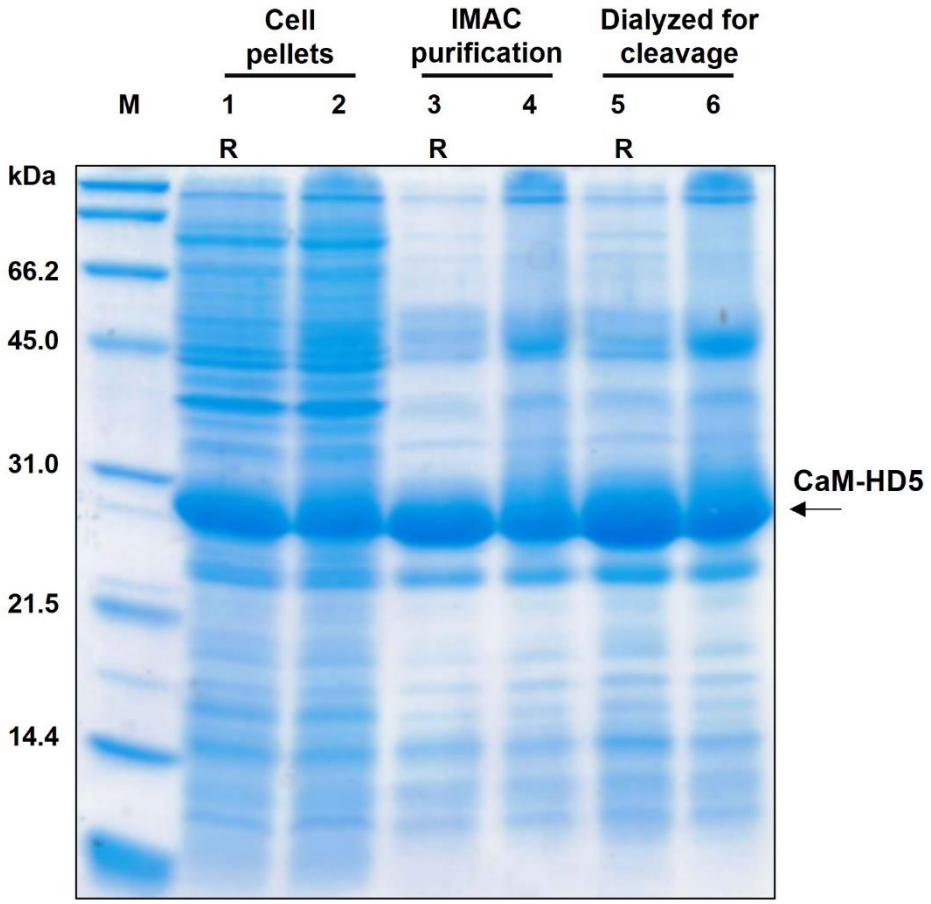

Fig. 2. SDS-PAGE analysis of the purification process of ^{15}N-labeled CaM-HD5. Lane M: Molecular weight marker; Lanes 1–2: Supernatant obtained after centrifugation of sonicated BL21(DE3) cell pellets. Lanes 3–4: Main elution from IMAC purification, eluted with 300 mM imidazole. Lanes 5–6: Supernatant after centrifugation of the Tris-HCl buffer (pH 8.0)-dialyzed sample prepared for EK digestion. R: Samples reduced with β-mercaptoethanol before loading onto the gel.

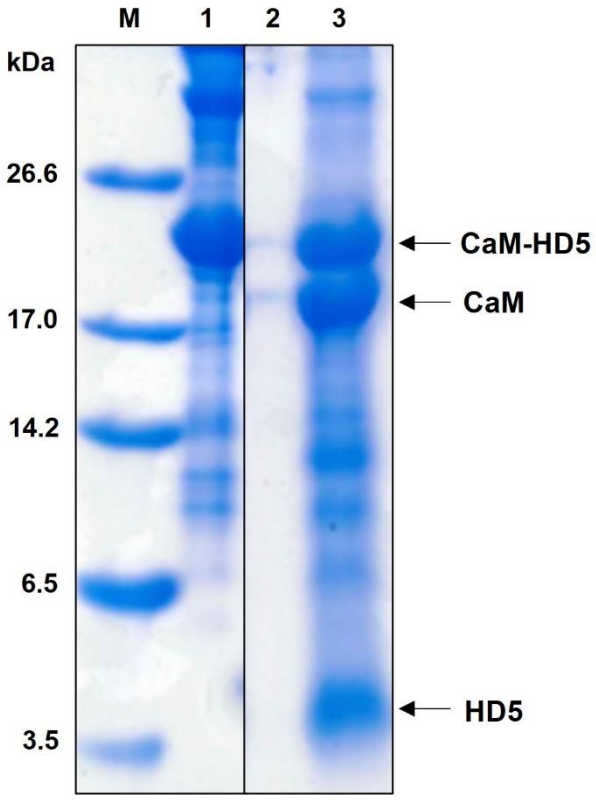

Fig. 3. Tricine SDS-PAGE analysis of EK digestion under optimal conditions. Lane M: Molecular weight marker; Lane 1: Intact CaM-HD5 fusion protein before cleavage. Lanes 2–3: Pellet and supernatant after centrifugation of the EK-treated mixture, respectively.

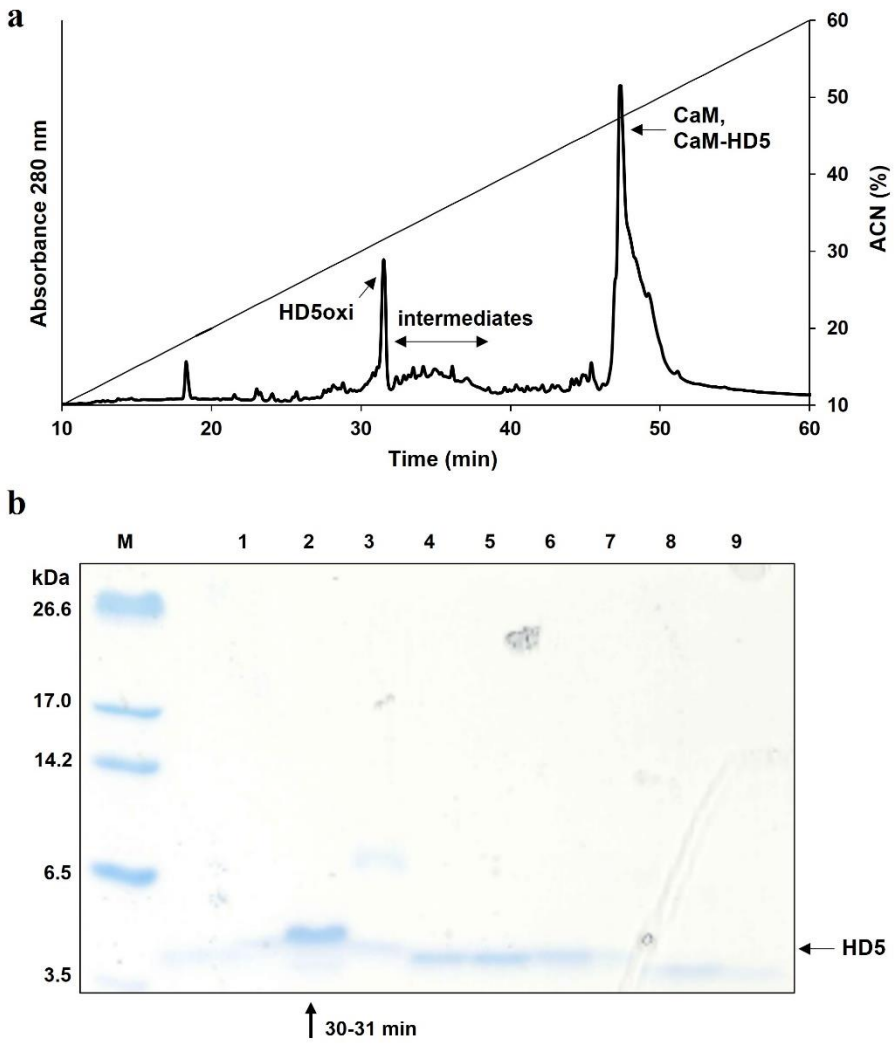

Fig. 4. Purification of HD5 after EK digestion by RP-HPLC. (**a**) RP-HPLC chromatogram of EK-treated samples using a 10–60% ACN gradient containing 0.1% TFA. The HD5oxi peak appears at 30–31 minutes, while HD5-related intermediates elute between 31–37 minutes. Cleaved CaM and intact CaM–HD5 fusion proteins exhibit overlapping peaks at 47–50 minutes. (**b**) Tricine SDS-PAGE analysis of RP-HPLC fractions collected between 29.5 and 37 minutes. Lane M: Molecular weight marker; Lanes 1–9: Fractions corresponding to 29.5–30 min, 30–31 min, 31.5–32 min, 32–32.5 min, 32.5–33 min, 33–34 min, 34–34.5 min, 35–36 min, and 36–37 min, respectively.

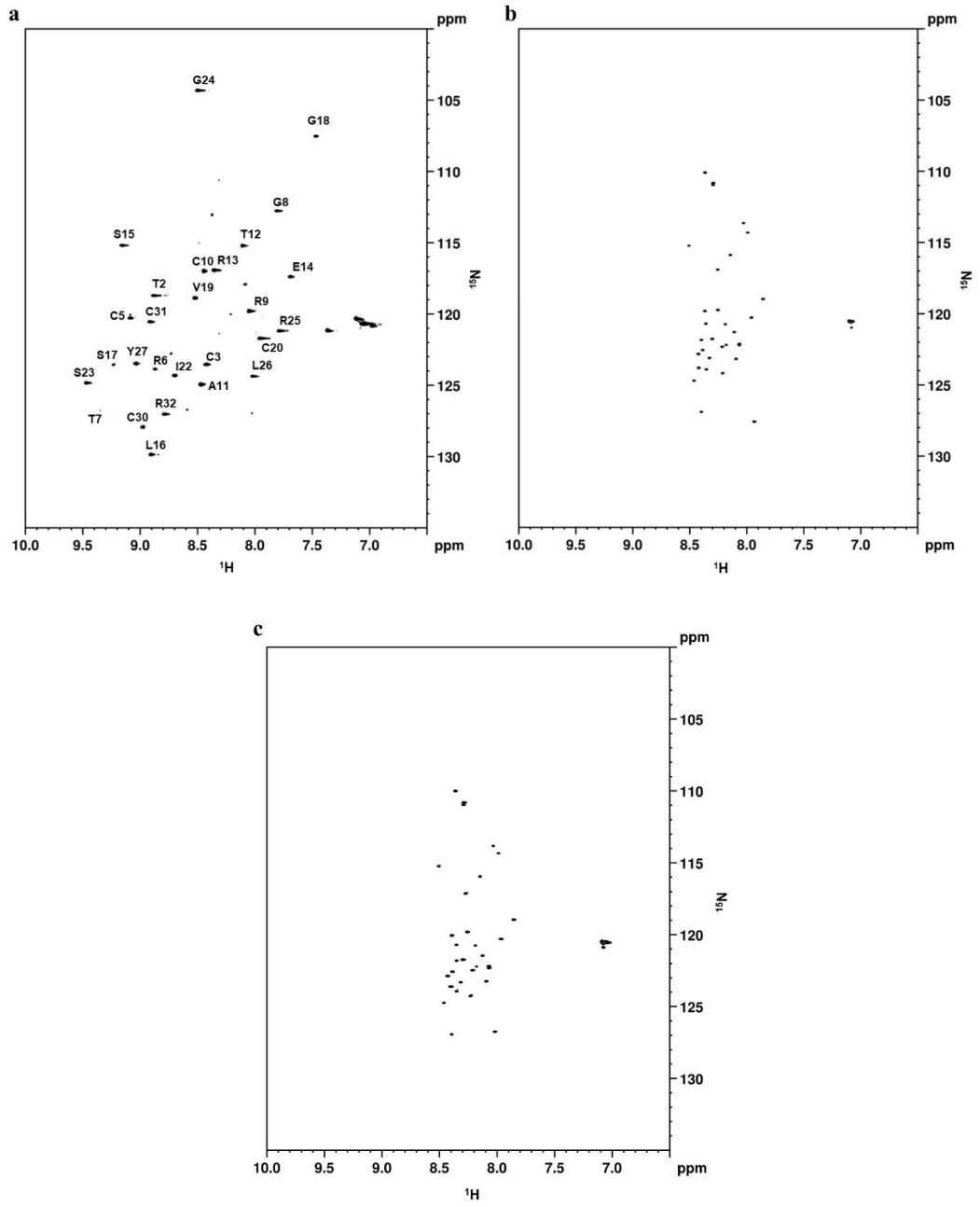

Fig. 5. ^{1}H–^{15}N HSQC spectra of recombinant HD5. (**a**) Spectrum of ^{15}N-labeled HD5oxi with backbone amide signal assignments. (**b**) Spectrum of ^{15}N-labeled HD5red. Lyophilized peptide samples were dissolved in sterile water containing 10% D_2O (pH 4.0) at a concentration of 0.2 mM. (**c**) Spectrum of ^{15}N-labeled HD5red mixed with non-labeled CaM at a 1:1 molar ratio in aqueous solution.

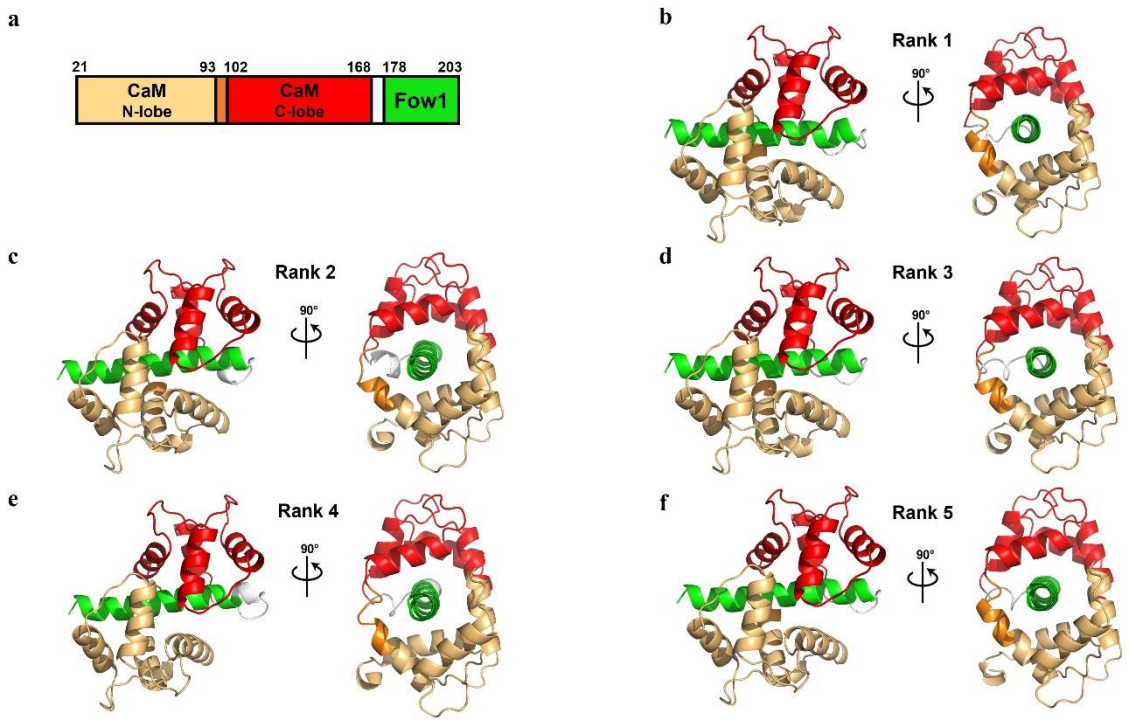

Fig. 6. Structural prediction of the CaM-Fow1 fusion protein. (**a**) Schematic representation of each region of the fusion protein. The N-terminal His-tag region is omitted. (**b–f**) Structural models predicted by AlphaFold, shown in order of rank. Figures were generated using PyMOL software.

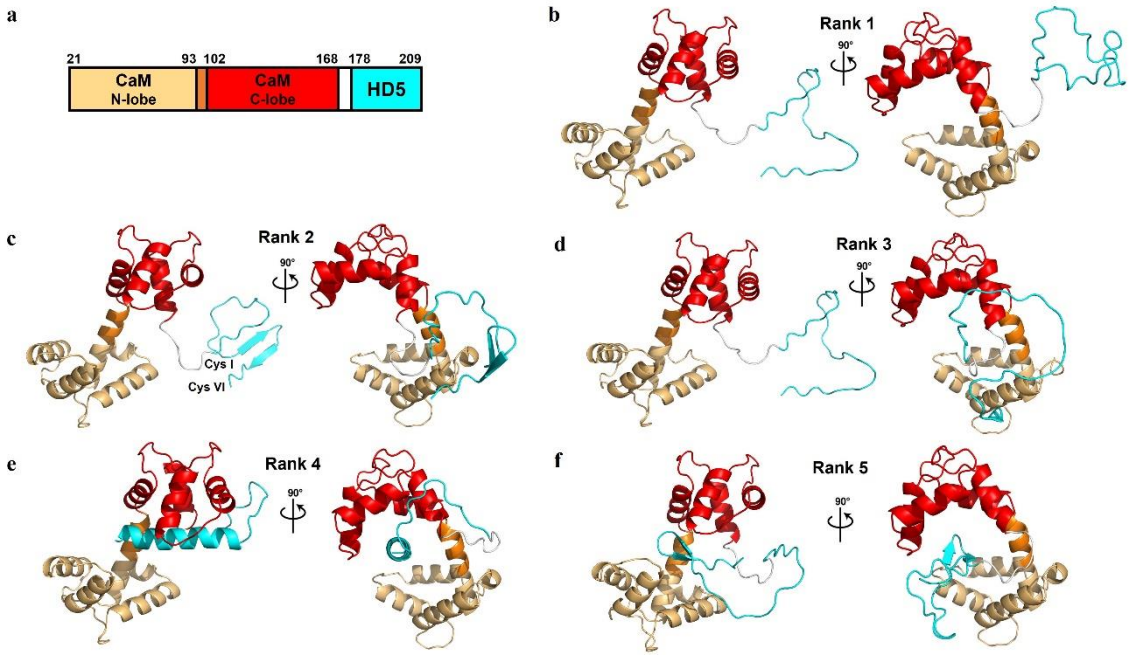

Fig. 7. Structural prediction of the CaM-HD5 fusion protein. (**a**) Schematic representation of each region of the fusion protein. The N-terminal His-tag region is omitted. (**b–f**) Structural models predicted by AlphaFold, shown in order of rank. Figures were generated using PyMOL software.

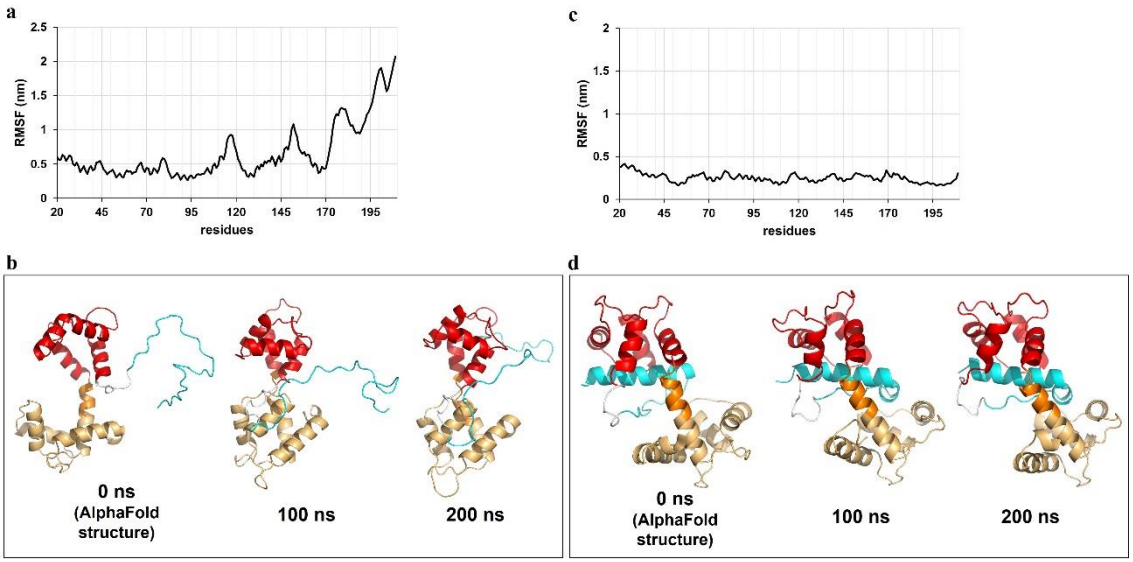

Fig. 8. MD simulation of the CaM-HD5 structure. (**a, c**) RMSF values from 200 ns MD simulations starting from the rank 1 predicted structure (**a**) and the rank 4 predicted structure (**c**). The plots depict RMSF values (y-axis) for each residue position (x-axis). (**b, d**) Structural comparison of MD simulations starting from the rank 1 structure (**b**) and the rank 4 structure (**d**) across different time points. Structures were visualized using PyMOL software.

Table 1 Characteristics of HD5 and CaM

Proteins	Mw (g/mol)	PI	GRAVY score	Charge
HD5	3,588.18	8.96	-0.11	+3.36
CaM	16,837.42	4.09	-0.65	-23.96

Molecular weight (Mw), isoelectric point (PI), grand average of hydropathy (GRAVY).

Calculated by Peptide Calculator Tool, BIOSYNTH®.

Table 2 Characterization of HD5 after RP-HPLC purification

	Retention time (min) in RP-HPLC	Calculated Mw (g/mol)	Observed Mw (g/mol)
^{15}N-HD5oxi	30-31	3631.75	3631.46
^{15}N-HD5red	39	3637.81	3637.39

Table 3 Minimal inhibitory concentrations (MIC) of recombinant HD5oxi

Microorganism	MIC (μM) (n=3)
Gram positive	
S. aureus (ATCC6538p)	1
Gram negative	
E. coli (ATCC43827)	4

Each MIC was determined from three independent replicates.

7. Supplement materials

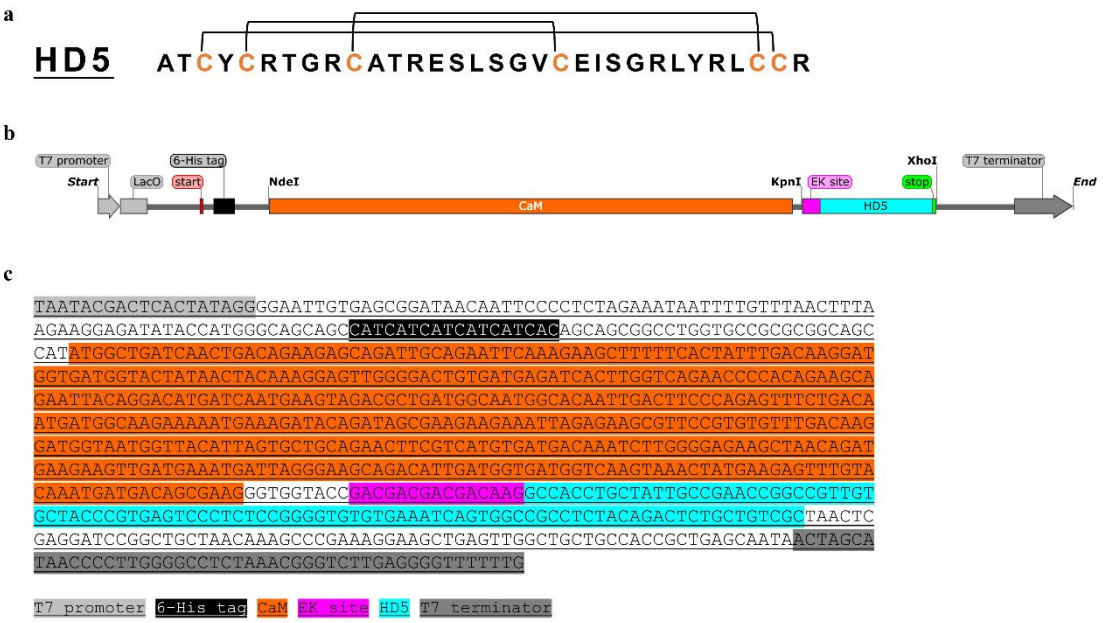

Fig. S1. **Sequence information.** (**a**) Amino acid sequence of HD5. Cysteine residues are highlighted in orange. (**b**) Schematic representation of the pCaM-EK-HD5 expression vector. The map was generated using SnapGene software (www.snapgene.com). (**c**) DNA sequence of the expression region of the pCaM-EK-HD5 vector.

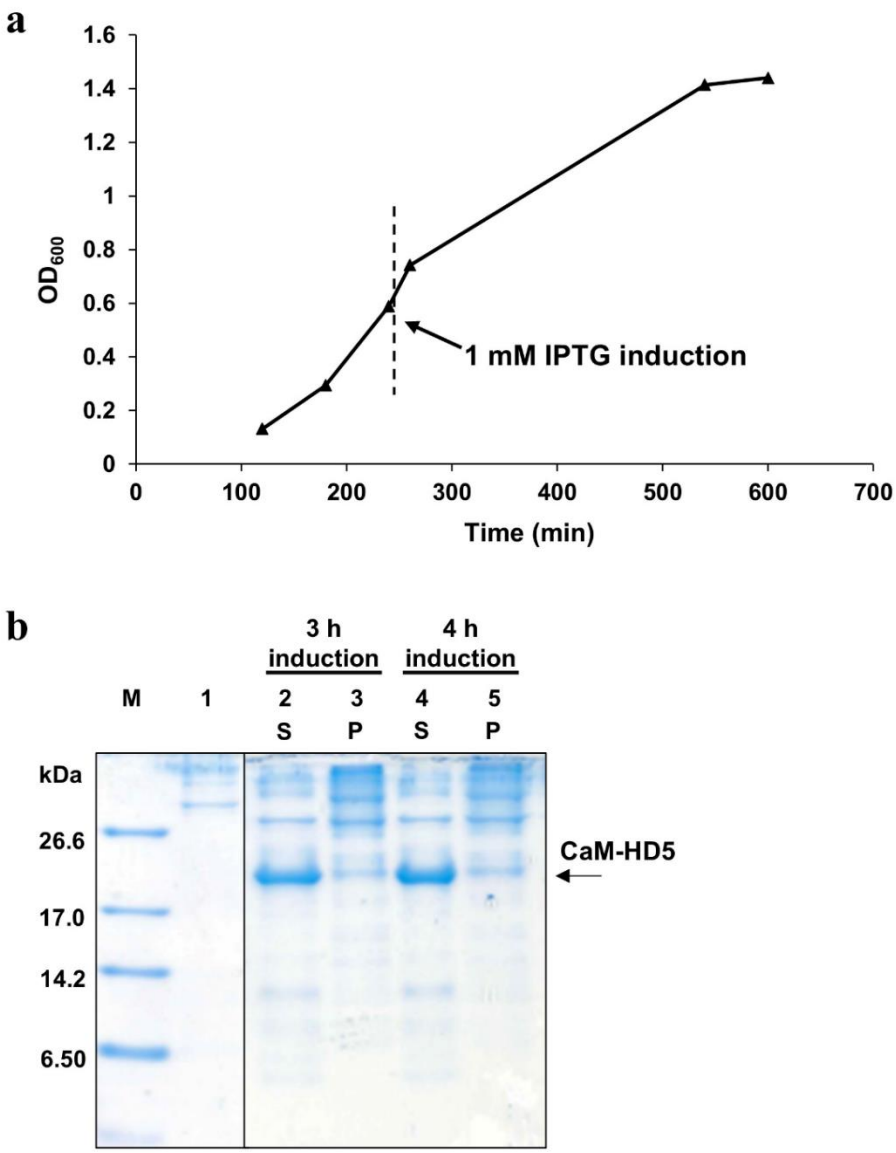

Fig. S2. Overexpression of ^{15}N, ^{13}C-labeled CaM-HD5. (**a**) Growth curve of *E. coli* BL21(DE3) cells expressing ^{15}N, ^{13}C-CaM-HD5 in M9 medium, induced with 1 mM IPTG at an OD_{600} of 0.6–0.8. (**b**) Tricine SDS-PAGE analysis of lysed cell pellets induced with 1 mM IPTG. Lane M: Molecular weight marker; Lane 1: Whole cells before induction; Lanes 2–3: Supernatant and pellet after centrifugation of lysed cells following 3 h of induction, respectively; Lanes 4–5: Supernatant and pellet after centrifugation of lysed cells following 4 h of induction, respectively.

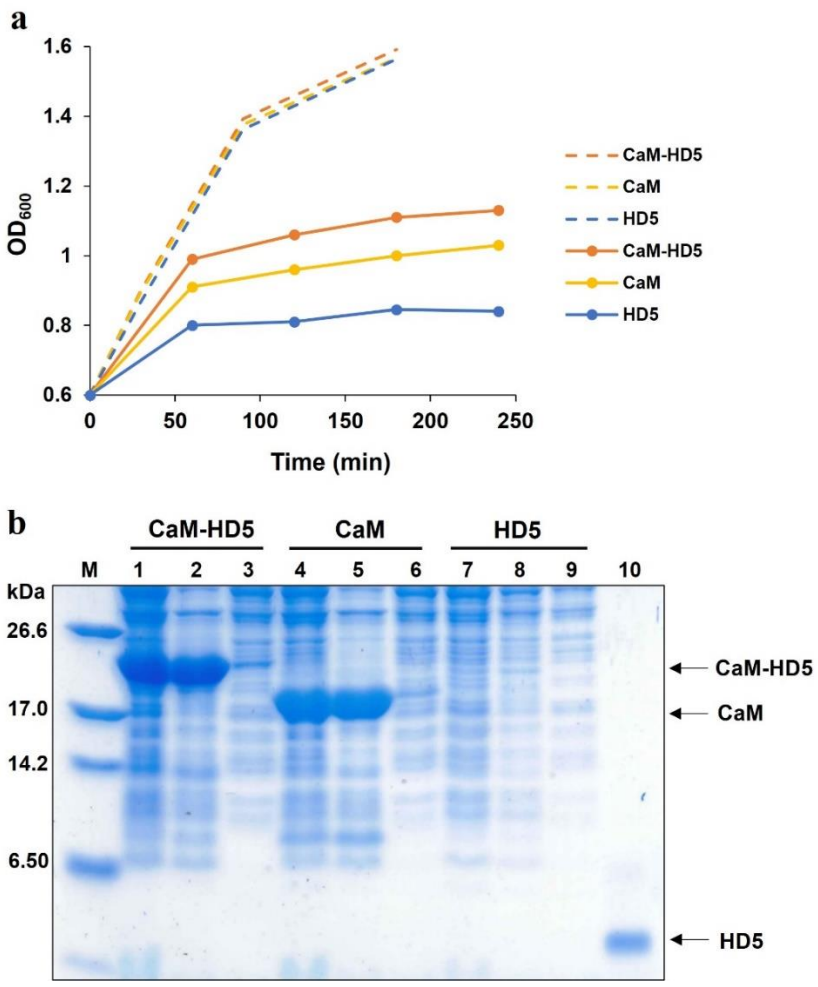

Fig. S3. A comparison of cultivation and overexpression of CaM-HD5 fusion, CaM and HD5 constructs. (**a**) Growth curve of *E. coli* BL21(DE3) cells expressing CaM-HD5 (orange), CaM (yellow) and HD5 (blue) in LB medium, induced with 1 mM IPTG at OD_{600} of 0.6. The growth curves of each construct cultivated without IPTG induction are shown as dashed lines. (**b**) Tricine SDS-PAGE analysis of each construct after IPTG induction. Lane M: Molecular weight marker; Lanes 1, 4, 7: The whole lysed cells of CaM-HD5, CaM and HD5 construct, respectively; Lanes 2, 5, 8: Supernatant after centrifugation; Lanes 3, 6, 9: Precipitation resuspended by Tris-HCl buffer (pH 8.0); Lane 10: standard HD5 (control).

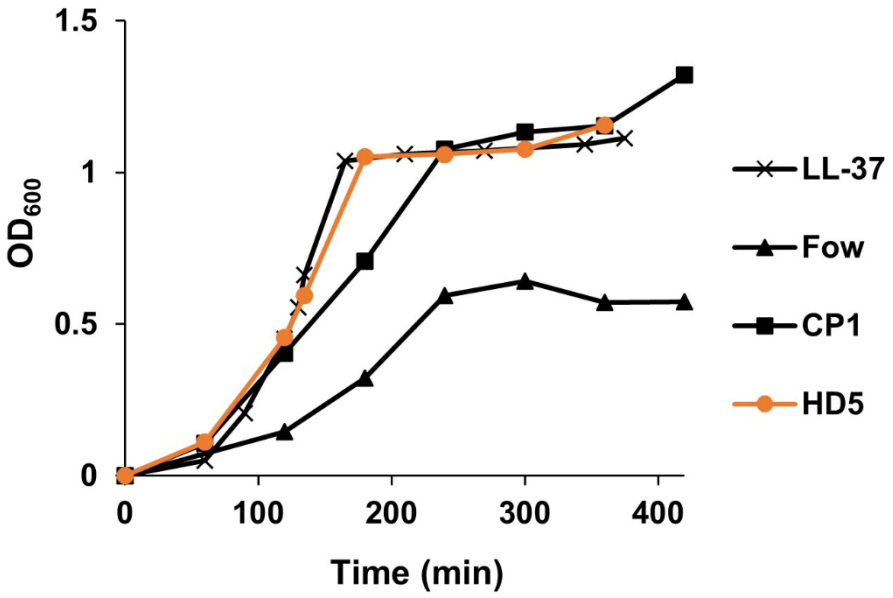

Fig. S4. The effect of AMPs fused with CaM on the growth of *E. coli* BL21 (DE3). Growth curves of IPTG-induced expression for CaM-LL37 (X-shaped markers), CaM-Fow1 (Fow) (triangle markers), CaM-CP1 (square markers), and CaM-HD5 (orange line, circle markers) are shown. Cells were cultivated in test tubes containing LB medium at 37°C and induced with 1 mM IPTG when the OD_{600} reached 0.6–0.8. The expression vectors were constructed using the same method as for pCaM-EK-HD5.

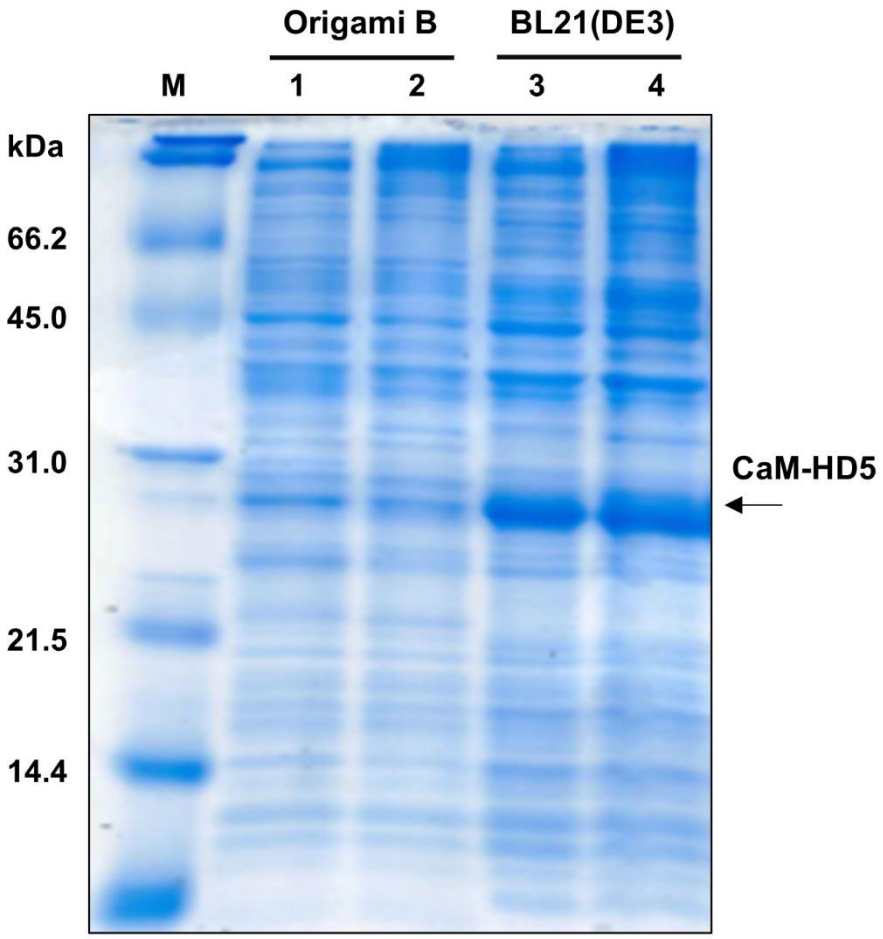

Fig. S5. Overexpression of CaM-HD5 in *E. coli* Origami B (DE3) and BL21 (DE3) strains as shown by SDS-PAGE analysis. Lane M: Molecular weight marker; Lanes 1–2: Supernatant from lysed Origami B cell pellets induced with 1 mM IPTG for 3 h and 4 h, respectively; Lanes 3–4: Supernatant from lysed BL21 cell pellets induced with 1 mM IPTG for 3 h and 4 h, respectively.

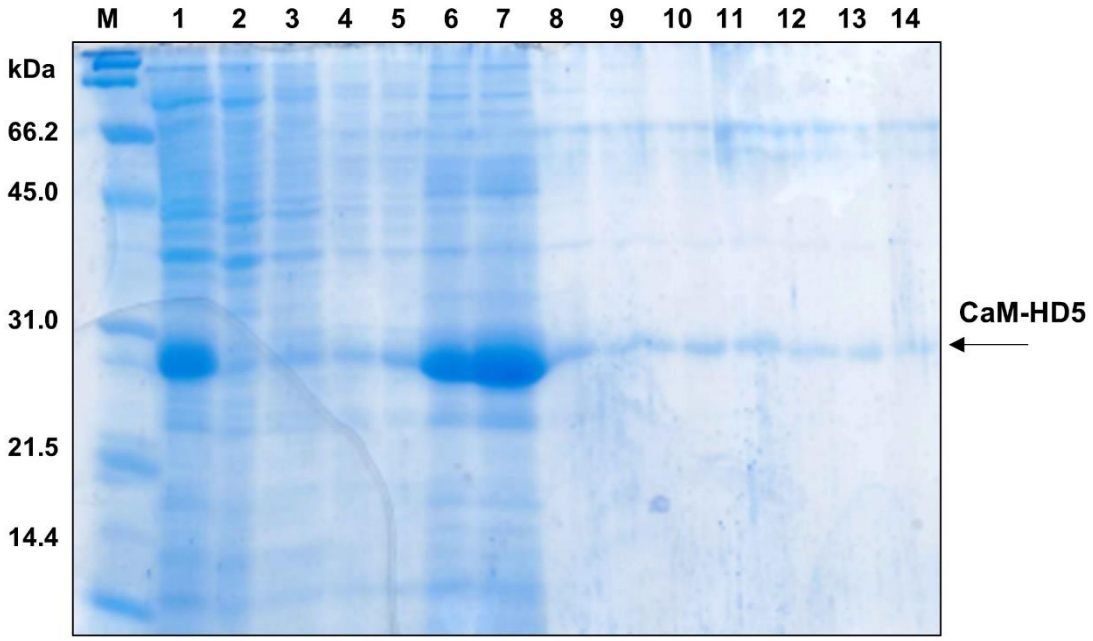

Fig. S6. IMAC purification of CaM-HD5 shown by SDS-PAGE analysis. Lane M: Molecular weight marker; Lane 1: Supernatant from lysed BL21 cell pellets induced with 1 mM IPTG for 4 h (positive control); Lane 2: Flow-through from loading sample onto the Ni^{2+}-NTA column; Lane 3: Wash-out from washing the column with a buffer containing 20 mM Tris-HCl, 300 mM NaCl, and 20 mM imidazole (pH 8.0); Lanes 4–13: Elution with a buffer containing 300 mM imidazole; Lane 14: Final elution with a buffer containing 500 mM imidazole.

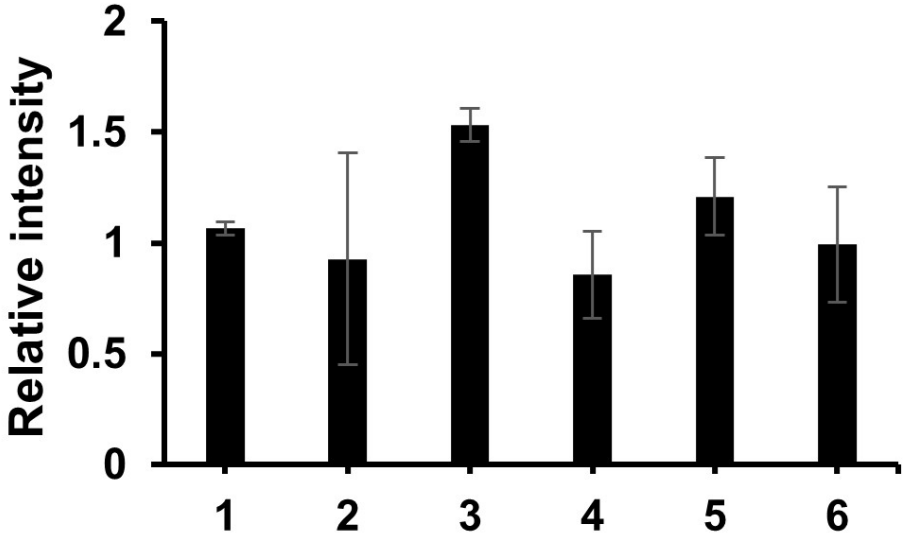

Fig. S7. Relative intensity of recovered HD5 under various reaction conditions of EK digestion. Each bar represents the following conditions: 1–2: 0.5 U/mL EK, 20 h reaction at 22°C and 30°C, respectively; 3–4: 1 U/mL EK, 20 h reaction at 22°C and 30°C, respectively; 5–6: 0.5 U/mL and 1 U/mL EK, respectively, at 22°C for 24 h.

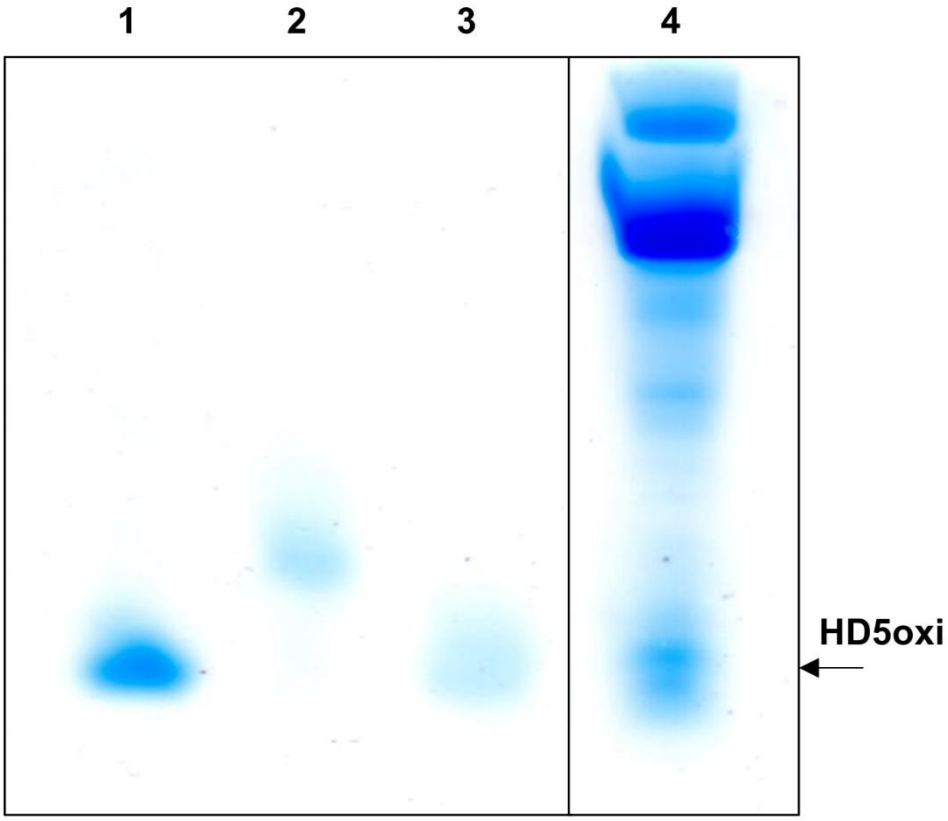

Fig. S8. AU-PAGE of recombinant HD5oxi. Lane 1: Chemically synthesized HD5oxi; Lane 2: Chemically synthesized HD5oxi treated with DTT; Lane 3: Recombinant HD5oxi from the current overexpression and purification system; Lane 4: Fusion protein sample after EK digestion. The samples were mixed with 3× AU-PAGE buffer (15% acetic acid with 30% glycerol dissolved in water) at a 2:1 volume ratio.

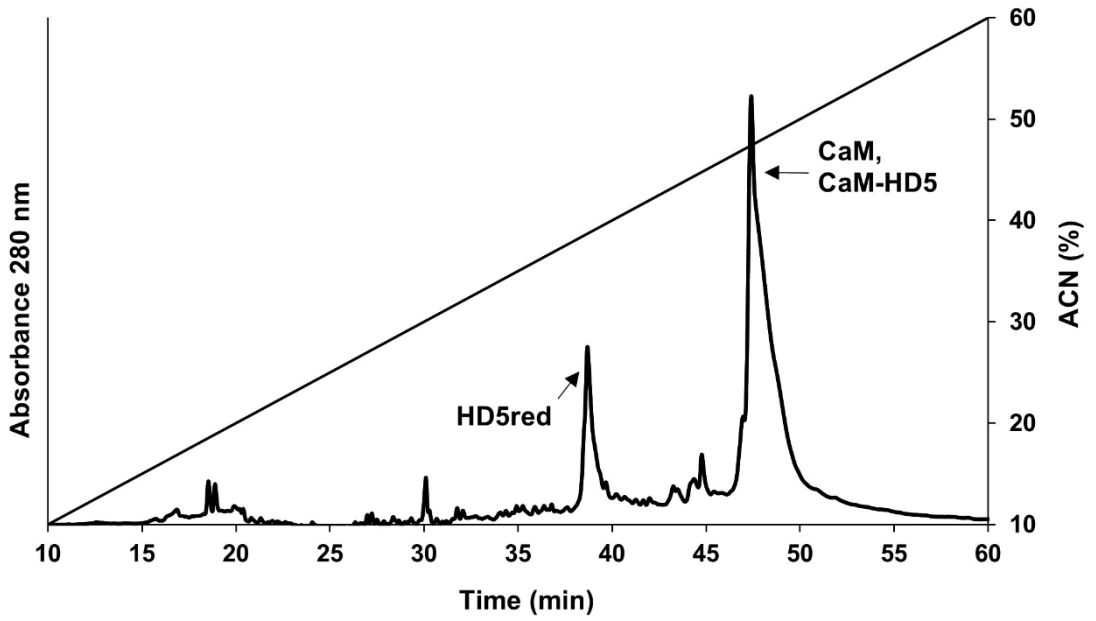

Fig. S9. Purification of HD5red by RP-HPLC. The EK-treated samples reduced with DTT were eluted with a 10–60% ACN gradient containing 0.1% TFA. The HD5red peak appears around 39 minutes. The cleaved CaM and intact CaM–HD5 fusion proteins exhibit overlapping peaks at 47–50 minutes.

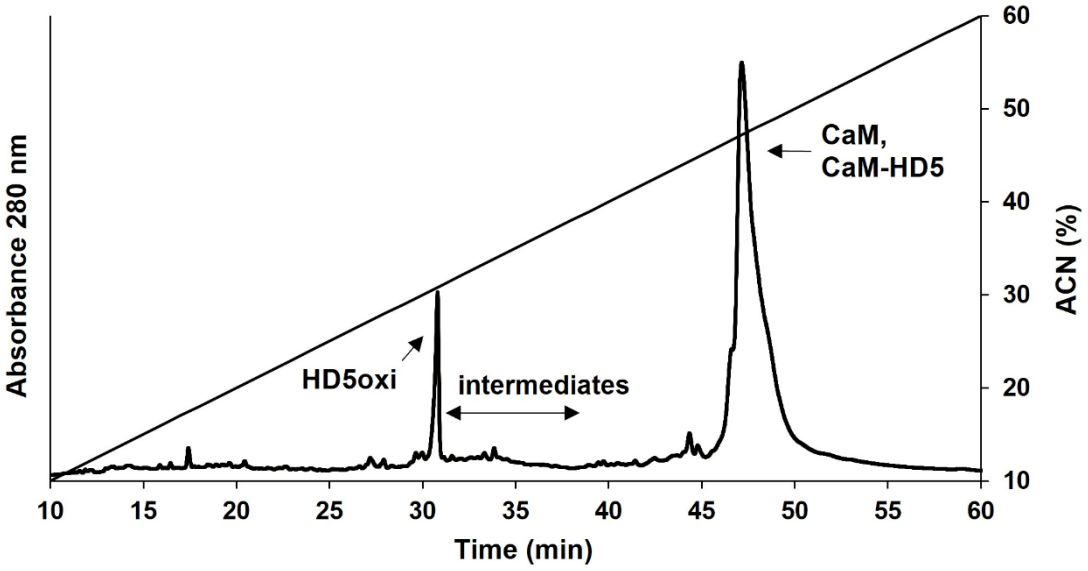

Fig. S10. Purification of HD5 after refolding and EK digestion by RP-HPLC. Samples were eluted with a 10–60% ACN gradient containing 0.1% TFA. The HD5oxi peak appears at 30–31 minutes, while decreased HD5-related intermediates elute between 31 and 37 minutes. The cleaved CaM and intact CaM–HD5 fusion proteins exhibit overlapping peaks at 47–50 minutes.

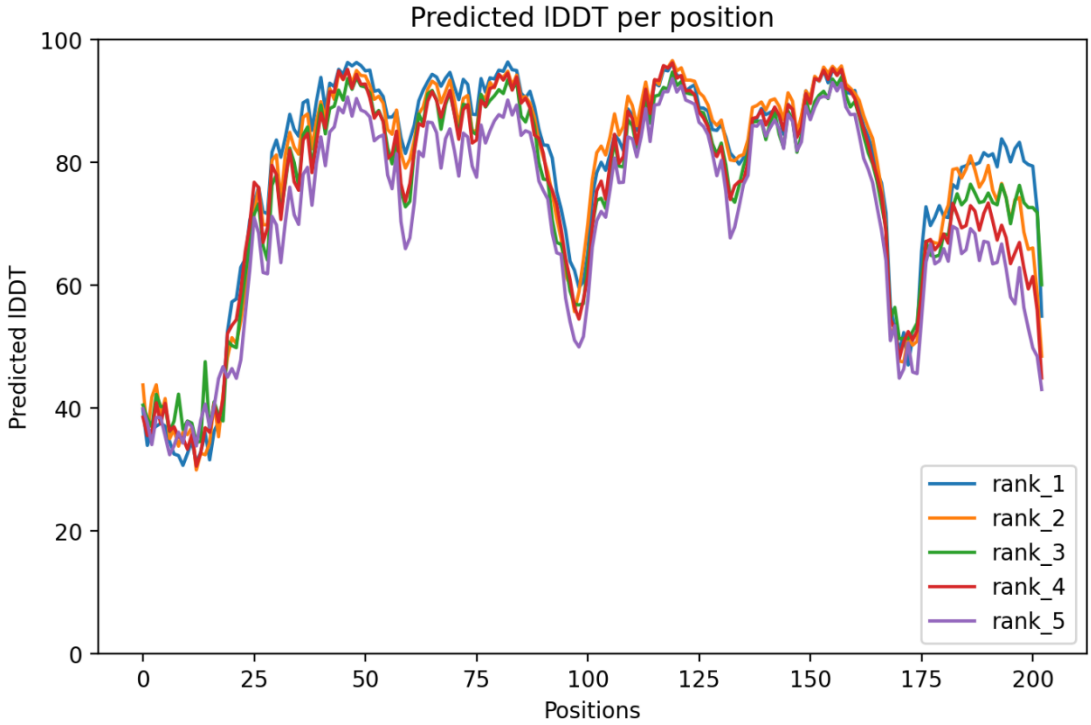

Fig. S11. pLDDT score for the CaM-Fow1 structure predicted by AlphaFold. The plot shows the pLDDT scores for each residue position across five ranked models (rank 1 to rank 5), output from the Colab server. The x-axis represents the residue positions, and the y-axis indicates the pLDDT score (0–100), with higher scores reflecting greater confidence in the predicted local structure.

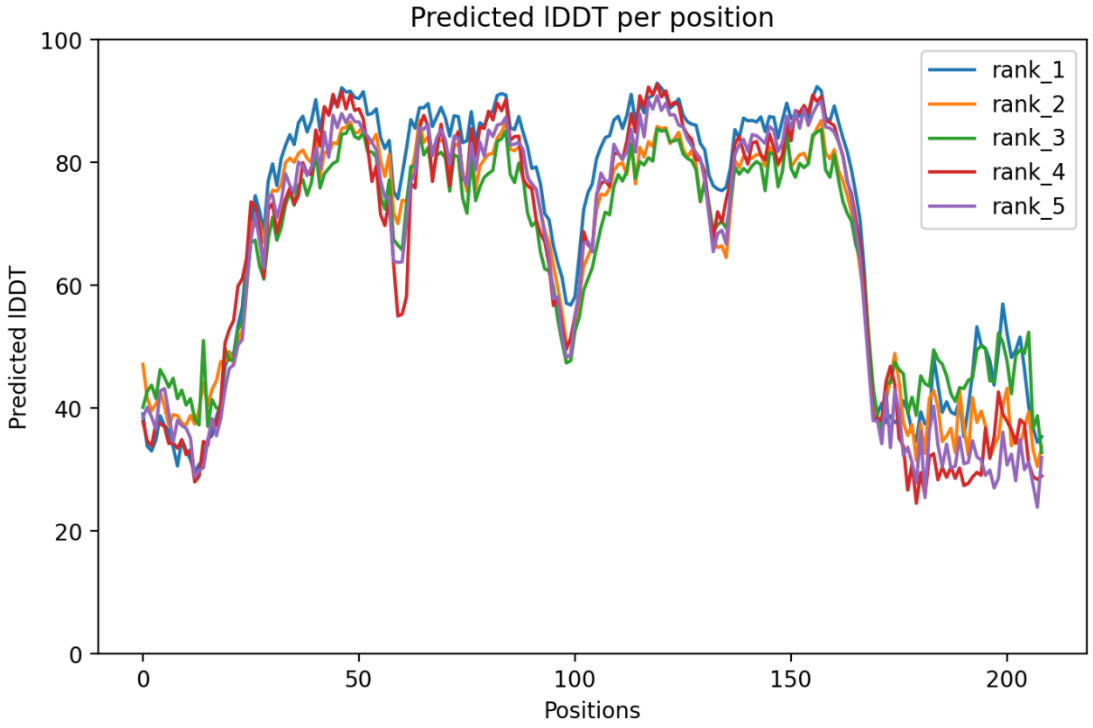

Fig. S12. pLDDT score for the CaM-HD5 structure predicted by AlphaFold. The plot shows the pLDDT scores for each residue position across five ranked models (rank 1 to rank 5), output from the Colab server. The x-axis represents the residue positions, and the y-axis indicates the pLDDT score (0–100), with higher scores reflecting greater confidence in the predicted local structure.

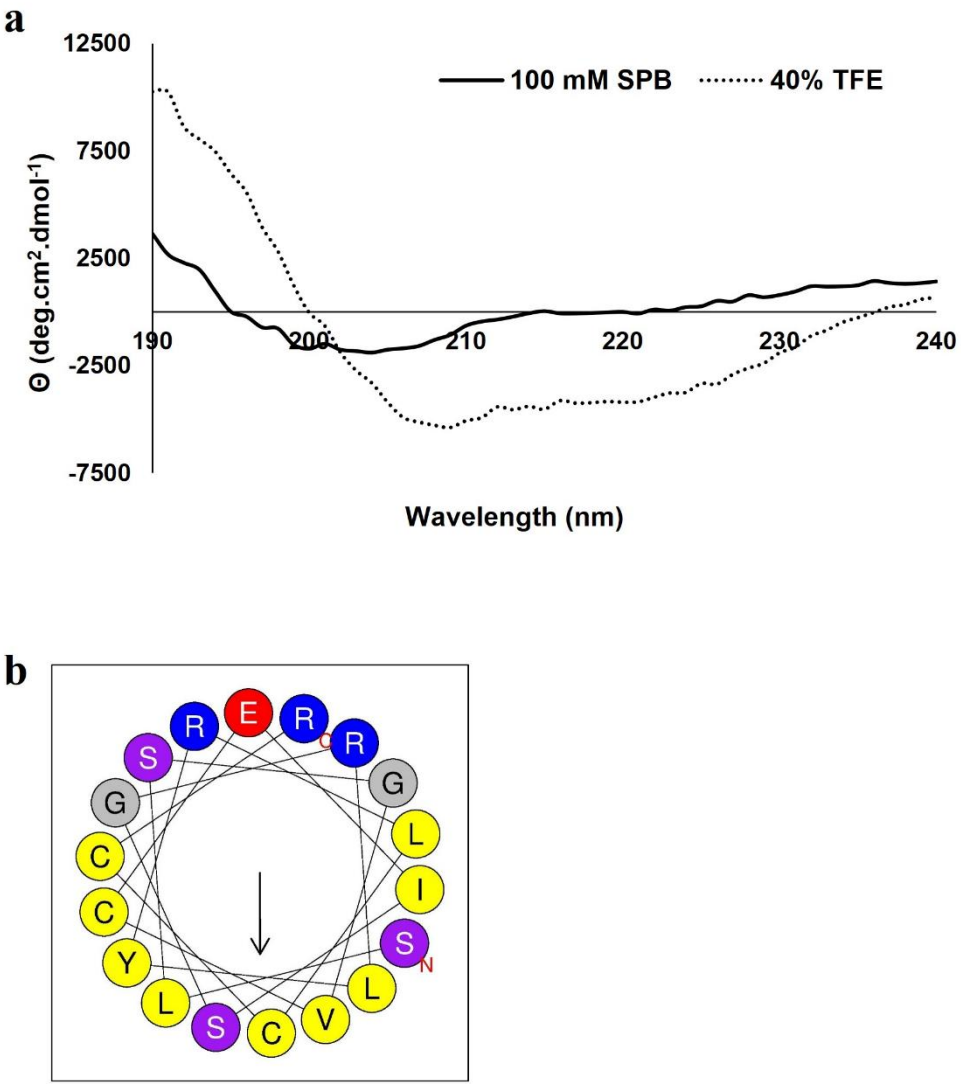

Fig. S13. Secondary structure analysis of HD5 by circular dichroism (CD) spectra. (**a**) CD spectra measured from 240 to 190 nm at 25°C. Each sample containing 27.8 μM of HD5red peptides was measured in 10 mM sodium phosphate buffer (pH 7.4) (black lines) and in 40% trifluoroethanol (TFE) (short-dashed lines). (**b**) Helical-wheel diagrams of the C-terminal region of HD5 (Ser15 to Arg32) using HeliQuest. Positively charged amino acid residues are shown in blue, negatively charged residues in red, hydrophobic residues in yellow, and Gly in gray. The arrow indicates the helical hydrophobic moment.

Acknowledgements

This work was partially supported by the grants JPMJPF2108 from the Center of Innovation NEXT Program and JPMJSP2119 from SPRING Program of the Japan Science and Technology Agency.

References

[1] R. I. Lehrer, “Primate defensins,” *Nat. Rev. Microbiol.*, vol. 2, no. 9, pp. 727–738, 2004, doi: 10.1038/nrmicro976.

[2] T. Ganz, “Defensins: Antimicrobial peptides of innate immunity,” *Nat. Rev. Immunol.*, vol. 3, no. 9, pp. 710–720, 2003, doi: 10.1038/nri1180.

[3] X. Gao, J. Ding, C. Liao, J. Xu, X. Liu, and W. Lu, “Defensins: The natural peptide antibiotic,” *Adv. Drug Deliv. Rev.*, vol. 179, p. 114008, 2021, doi: 10.1016/j.addr.2021.114008.

[4] T. Ganz *et al.*, “Defensins. Natural peptide antibiotics of human neutrophils,” *J. Clin. Invest.*, vol. 76, no. 4, pp. 1427–1435, 1985, doi: 10.1172/JCI112120.

[5] K. Nakamura, N. Sakuragi, A. Takakuwa, and T. Ayabe, “Paneth cell α-defensins and enteric microbiota in health and disease,” *Biosci. Microbiota, Food Heal.*, vol. 35, no. 2, pp. 57–67, 2016, doi: 10.12938/bmfh.2015-019.

[6] G. Wang, “Human antimicrobial peptides and proteins,” *Pharmaceuticals*, vol. 7, no. 5, pp. 545–594, 2014, doi: 10.3390/ph7050545.

[7] O. Scudiero, M. Brancaccio, C. Mennitti, S. Laneri, R. Colicchio, and P. Salvatore, “Human Defensins : A Novel Approach in the Fight against Skin Colonizing Staphylococcus aureus,” *Antibiotics*, vol. 9, pp. 1–16, 2020, doi: 10.3390/antibiotics9040198.

[8] C. Wang *et al.*, “Reduction Impairs the Antibacterial Activity but Benefits the LPS

Neutralization Ability of Human Enteric Defensin 5," *Sci. Rep.*, vol. 6, no. February, pp. 1–12, 2016, doi: 10.1038/srep22875.

[9] B. Ericksen, Z. Wu, W. Lu, and R. I. Lehrer, "Antibacterial activity and specificity of the six human α-defensins," *Antimicrob. Agents Chemother.*, vol. 49, no. 1, pp. 269–275, 2005, doi: 10.1128/AAC.49.1.269-275.2005.

[10] A. J. Wommack *et al.*, "NMR solution structure and condition-dependent oligomerization of the antimicrobial peptide human defensin 5," *Biochemistry*, vol. 51, no. 48, pp. 9624–9637, Dec. 2012, doi: 10.1021/bi301255u.

[11] D. E. Jones and C. L. Bevins, "Paneth cells of the human small intestine express an antimicrobial peptide gene," *J. Biol. Chem.*, vol. 267, no. 32, pp. 23216–23225, 1992, doi: 10.1016/s0021-9258(18)50079-x.

[12] D. Elphick, S. Liddell, and Y. R. Mahida, "Impaired luminal processing of human defensin-5 in Crohn's disease: Persistence in a complex with chymotrypsinogen and trypsin," *Am. J. Pathol.*, vol. 172, no. 3, pp. 702–713, 2008, doi: 10.2353/ajpath.2008.070755.

[13] P. Chairatana, J. Niramitranon, and P. Pongprayoon, "Dynamics of human defensin 5 (HD5) self-assembly in solution: Molecular simulations/insights," *Comput. Biol. Chem.*, vol. 83, no. July, p. 107091, 2019, doi: 10.1016/j.compbiolchem.2019.107091.

[14] Y. A. Wanniarachchi, P. Kaczmarek, A. Wan, and E. M. Nolan, "Human defensin 5 disulfide array mutants: Disulfide bond deletion attenuates antibacterial activity

against staphylococcus aureus," *Biochemistry*, vol. 50, no. 37, pp. 8005–8017, 2011, doi: 10.1021/bi201043j.

[15] Y. Zhang, F. B. L. Cougnon, Y. A. Wanniarachchi, J. A. Hayden, and E. M. Nolan, "Reduction of human defensin 5 affords a high-affinity zinc-chelating peptide," *ACS Chem. Biol.*, vol. 8, no. 9, pp. 1907–1911, 2013, doi: 10.1021/cb400340k.

[16] D. Ehmann *et al.*, "Paneth cell α-defensins HD-5 and HD-6 display differential degradation into active antimicrobial fragments," *Proc. Natl. Acad. Sci. U. S. A.*, vol. 116, no. 9, pp. 3746–3751, 2019, doi: 10.1073/pnas.1817376116.

[17] H. P. Sørensen and K. K. Mortensen, "Advanced genetic strategies for recombinant protein expression in Escherichia coli," *J. Biotechnol.*, vol. 115, no. 2, pp. 113–128, 2005, doi: 10.1016/j.jbiotec.2004.08.004.

[18] Y. Li, "Recombinant production of antimicrobial peptides in Escherichia coli: A review," *Protein Expr. Purif.*, vol. 80, no. 2, pp. 260–267, 2011, doi: 10.1016/j.pep.2011.08.001.

[19] F. Baneyx and M. Mujacic, "Recombinant protein folding and misfolding in Escherichia coli," *Nat. Biotechnol.*, vol. 22, no. 11, pp. 1399–1407, 2004, doi: 10.1038/nbt1029.

[20] S. Lipničanová, B. Legerská, D. Chmelová, M. Ondrejovič, and S. Miertuš, "Optimization of an Inclusion Body-Based Production of the Influenza Virus Neuraminidase in Escherichia coli," *Biomolecules*, vol. 12, no. 2, p. 331, 2022, doi: 10.3390/biom12020331.

[21] Y. Li, “ Carrier proteins for fusion expression of antimicrobial peptides in Escherichia coli ,” *Biotechnol. Appl. Biochem.*, vol. 54, no. 1, pp. 1–9, 2009, doi: 10.1042/ba20090087.

[22] S. Deo, K. L. Turton, T. Kainth, A. Kumar, and H. J. Wieden, “Strategies for improving antimicrobial peptide production,” *Biotechnol. Adv.*, vol. 59, no. April, p. 107968, 2022, doi: 10.1016/j.biotechadv.2022.107968.

[23] A. J. McCluskey, G. M. K. Poon, and J. Gariépy, “A rapid and universal tandem-purification strategy for recombinant proteins,” *Protein Sci.*, vol. 16, no. 12, pp. 2726–2732, 2007, doi: 10.1110/ps.072894407.

[24] H. Ishida, L. T. Nguyen, R. Gopal, T. Aizawa, and H. J. Vogel, “Overexpression of Antimicrobial, Anticancer, and Transmembrane Peptides in Escherichia coli through a Calmodulin-Peptide Fusion System,” *J. Am. Chem. Soc.*, vol. 138, no. 35, pp. 11318–11326, Sep. 2016, doi: 10.1021/jacs.6b06781.

[25] Y. S. Babu, J. S. Sack, T. J. Greenhough, C. E. Bugg, A. R. Means, and W. J. Cook, “Three-dimensional structure of calmodulin,” *Nature*, vol. 315, no. 6014, pp. 37–40, 1985, doi: 10.1038/315037a0.

[26] Y. S. Babu, C. E. Bugg, and W. J. Cook, “Structure of calmodulin refined at 2.2 Å resolution,” *J. Mol. Biol.*, vol. 204, no. 1, pp. 191–204, 1988, doi: 10.1016/0022-2836(88)90608-0.

[27] L. A. Jurado, P. S. Chockalingam, and H. W. Jarrett, “Apocalmodulin,” vol. 79, no. 3, pp. 661–682, 2024.

[28] M. Zhang and H. J. Vogel, “Characterization of the calmodulin-binding domain of rat cerebellar nitric oxide synthase,” *J. Biol. Chem.*, vol. 269, no. 2, pp. 981–985, 1994, doi: 10.1016/s0021-9258(17)42208-3.

[29] H. Gu *et al.*, “Three-Dimensional Structure of the Antimicrobial Peptide Cecropin P1 in Dodecylphosphocholine Micelles and the Role of the C - Terminal Residues,” 2022, doi: 10.1021/acsomega.2c02778.

[30] G. Ramamourthy, M. Arias, L. T. Nguyen, H. Ishida, and H. J. Vogel, “Expression and purification of chemokine mip-3α (Ccl20) through a calmodulin-fusion protein system,” *Microorganisms*, vol. 7, no. 1, Jan. 2019, doi: 10.3390/microorganisms7010008.

[31] Y. Wang *et al.*, “Antimicrobial Properties and Mode of Action of Cryptdin-4, a Mouse α-Defensin Regulated by Peptide Redox Structures and Bacterial Cultivation Conditions,” *Antibiotics*, vol. 12, no. 6, 2023, doi: 10.3390/antibiotics12061047.

[32] Y. Song *et al.*, “Efficient recombinant production of mouse-derived cryptdin family peptides by a novel facilitation strategy for inclusion body formation,” *Microb. Cell Fact.*, vol. 22, no. 1, p. 9, Jan. 2023, doi: 10.1186/s12934-023-02016-2.

[33] A. Wang *et al.*, “High level expression and purification of bioactive human α-defensin 5 mature peptide in Pichia pastoris,” *Appl. Microbiol. Biotechnol.*, vol. 84, no. 5, pp. 877–884, 2009, doi: 10.1007/s00253-009-2020-x.

[34] J. M. Kim, S. A. Jang, B. J. Yu, B. H. Sung, J. H. Cho, and S. C. Kim, “High-level expression of an antimicrobial peptide histonin as a natural form by multimerization and furin-mediated cleavage,” *Appl. Microbiol. Biotechnol.*, vol. 78, no. 1, pp. 123–130, 2008, doi: 10.1007/s00253-007-1273-5.

[35] M. Mirdita, K. Schütze, Y. Moriwaki, L. Heo, S. Ovchinnikov, and M. Steinegger, “ColabFold: making protein folding accessible to all,” *Nat. Methods*, vol. 19, no. 6, pp. 679–682, 2022, doi: 10.1038/s41592-022-01488-1.

[36] D. Van Der Spoel, E. Lindahl, B. Hess, G. Groenhof, A. E. Mark, and H. J. C. Berendsen, “GROMACS: Fast, flexible, and free,” *J. Comput. Chem.*, vol. 26, no. 16, pp. 1701–1718, 2005, doi: 10.1002/jcc.20291.

[37] J. Lee *et al.*, “CHARMM-GUI Input Generator for NAMD, GROMACS, AMBER, OpenMM, and CHARMM/OpenMM Simulations Using the CHARMM36 Additive Force Field,” *J. Chem. Theory Comput.*, vol. 12, no. 1, pp. 405–413, 2016, doi: 10.1021/acs.jctc.5b00935.

[38] J. Huang *et al.*, “CHARMM36m: An improved force field for folded and intrinsically disordered proteins,” *Nat. Methods*, vol. 14, no. 1, pp. 71–73, 2016, doi: 10.1038/nmeth.4067.

[39] T. Darden, D. York, and L. Pedersen, “Particle mesh Ewald: An N·log(N) method for Ewald sums in large systems,” *J. Chem. Phys.*, vol. 98, no. 12, pp. 10089–10092, 1993, doi: 10.1063/1.464397.

[40] W. Humphrey, A. Dalke, and K. Schulten, “VMD: Visual Molecular Dynamics,”

J. Mol. Graph., vol. 14, no. October 1995, pp. 33–38, 1996, [Online]. Available: https://www.tapbiosystems.com/tap/products/index.htm.

[41] P. Diaz-Parga and E. de Alba, *Protein interactions of the inflammasome adapter ASC by solution NMR*, 1st ed., vol. 625. Elsevier Inc., 2019.

[42] J. Jumper *et al.*, "Highly accurate protein structure prediction with AlphaFold," *Nature*, vol. 596, no. 7873, pp. 583–589, 2021, doi: 10.1038/s41586-021-03819-2.

[43] S. W. Vetter and E. Leclerc, "Novel aspects of calmodulin target recognition and activation," *Eur. J. Biochem.*, vol. 270, no. 3, pp. 404–414, 2003, doi: 10.1046/j.1432-1033.2003.03414.x.

[44] C. Andrews, Y. Xu, M. Kirberger, and J. J. Yang, "Structural aspects and prediction of calmodulin-binding proteins," *Int. J. Mol. Sci.*, vol. 22, no. 1, pp. 1–26, 2021, doi: 10.3390/ijms22010308.

[45] K. L. Yap, J. Kim, K. Truong, M. Sherman, T. Yuan, and M. Ikura, "Calmodulin target database," *J. Struct. Funct. Genomics*, vol. 1, no. 1, pp. 8–14, 2000, doi: 10.1023/A:1011320027914.

[46] N. Juranic *et al.*, "Calmodulin wraps around its binding domain in the plasma membrane Ca 2+ pump anchored by a novel 18-1 motif," *J. Biol. Chem.*, vol. 285, no. 6, pp. 4015–4024, 2010, doi: 10.1074/jbc.M109.060491.

[47] A. López-Cano, M. Martínez-Miguel, J. Guasch, I. Ratera, A. Arís, and E. Garcia-Fruitós, "Exploring the impact of the recombinant Escherichia coli strain on defensins antimicrobial activity: BL21 versus Origami strain," *Microb. Cell Fact.*,

vol. 21, no. 1, pp. 1–10, 2022, doi: 10.1186/s12934-022-01803-7.

[48] N. Kaur, R. Dilawari, A. Kaur, G. Sahni, and P. Rishi, “Recombinant expression, purification and PEGylation of Paneth cell peptide (cryptdin-2) with value added attributes against Staphylococcus aureus,” *Sci. Rep.*, vol. 10, no. 1, pp. 1–14, 2020, doi: 10.1038/s41598-020-69039-2.

[49] S. Luo and N. B. Wehr, “Protein carbonylation: Avoiding pitfalls in the 2,4-dinitrophenylhydrazine assay,” *Redox Rep.*, vol. 14, no. 4, pp. 159–166, 2009, doi: 10.1179/135100009X392601.

[50] D. K. Mercer *et al.*, “Antimicrobial Susceptibility Testing of Antimicrobial Peptides to Better Predict Efficacy,” *Front. Cell. Infect. Microbiol.*, vol. 10, no. July, pp. 1–34, 2020, doi: 10.3389/fcimb.2020.00326.